



Article

Integrated Geophysical Imaging and Remote Sensing for Enhancing Geological Interpretation of Landslides with Uncertainty Estimation—A Case Study from Cisiec, Poland

Małgorzata Wróbel ¹, Iwona Stan-Kłeczek ¹, Artur Marciniak ^{2,*}, Mariusz Majdański ², Sebastian Kowalczyk ³, Adam Nawrot ² and Justyna Cader ⁴

¹ Faculty of Natural Sciences, University of Silesia, 41-200 Sosnowiec, Poland

² Institute of Geophysics, Polish Academy of Sciences, 01-452 Warszawa, Poland

³ Faculty of Geology, University of Warsaw, 02-089 Warszawa, Poland

⁴ Mineral and Energy Economy Research Institute, Polish Academy of Sciences, 31-261 Kraków, Poland

* Correspondence: amarciniak@igf.edu.pl

Abstract: Landslides, as one of the main problems in mountainous areas, are a challenging issue for modern geophysics. The triggers that cause these phenomena are diverse (including geological, geomorphological, and hydrological conditions, climatic factors, and earthquakes) and can occur in conjunction with each other. Human activity is also relevant, undoubtedly contributing to the intensification of landslide phenomena. One of these is the production of artificial snow on ski slopes. This paper presents a multimethod approach for imaging the landslide structure in Cisiec, in southwestern Poland, where such a situation occurs. In the presented work, the integration of remote sensing with multi-method geophysical imaging was used to visualize landslide zones, and to estimate ground motion. To verify the uncertainty of the obtained data, the combination of electrical resistivity tomography (ERT), multi-channel analysis of surface waves (MASW), and seismic refraction method (SRT) was supported by synthetic modeling. Using geophysical data with accurate GPS-based topography and a terrestrial laser scanning-based digital terrain model (DTM), it was possible to model the spatial variability and surface area of the landslide more precisely, as well as to estimate the velocity field in the nearest surface more accurately. The final result shows displacement up to 1 m on the ground surface visible on the DTM models, while the geophysical methods confirm the change in internal structure. The proposed methodology is fast, cost-effective, and can be used to image the structure of landslides, where the shallowest parts are usually complex and thus difficult to observe seismically.

Keywords: landslide; electrical resistivity tomography (ERT); seismic tomography; multichannel analysis of surface wave (MASW); digital terrain model (DTM); forward modeling



Citation: Wróbel, M.; Stan-Kłeczek, I.; Marciniak, A.; Majdański, M.; Kowalczyk, S.; Nawrot, A.; Cader, J. Integrated Geophysical Imaging and Remote Sensing for Enhancing Geological Interpretation of Landslides with Uncertainty Estimation—A Case Study from Cisiec, Poland. *Remote Sens.* **2023**, *15*, 238. <https://doi.org/10.3390/rs15010238>

Academic Editors: Hans-Balder Havenith, Romy Schlögel, Francesca Cigna, Veronica Pazzi and Marc-Henri Derron

Received: 23 November 2022

Revised: 29 December 2022

Accepted: 30 December 2022

Published: 31 December 2022



Copyright: © 2022 by the authors. Licensee MDPI, Basel, Switzerland. This article is an open access article distributed under the terms and conditions of the Creative Commons Attribution (CC BY) license (<https://creativecommons.org/licenses/by/4.0/>).

1. Introduction

Landslides are one of the main geohazards influenced by rapidly changing environmental factors [1,2]. Their development depends on the geological structure, topography, groundwater migration, and surface water activity [3]. Climatic changes and anthropogenic factors (e.g., land-use change, deforestation, expansion of human settlements) also cause ground movements [4]. Landslides occur mainly in regions with strongly undulating land surfaces, such as mountainous and upland areas, and may strongly endanger infrastructure and human life [5–7].

Compared to the rest of Europe, Poland is classified as not very prone to landslide processes—about 20% of the country's area may be considered relevant from this point of view, including mountainous regions, larger river valleys, the cliff coastline of the Baltic Sea, as well as areas covered by thick loess cover and with young glacial relief [8]. In particular, these are the mountain ranges, i.e., the Carpathians and the Sudetes, where

landslide susceptibility is described as medium and in some places as high [9]. Almost 62,000 landslides were identified in 2018, including 60,000 in the Carpathians, representing 9–10% of their area [10]. It is estimated that there may be as many as 100,000 landslides in Poland [9]. Globally, every year, landslides cause thousands of casualties and billions in monetary losses. In Poland, where more than 90% of the landslides occur in the Carpathian region [10,11], studies of that leading problem are necessary to assuring both the safety of the infrastructure and that of human existence.

Due to its nature, the study of landslides is difficult and requires precise imaging and modeling over time [12]. The characteristics of landslide areas can be very diverse, which makes it highly problematic to develop general rules for their identification [13,14]. Particularly challenging is the complex geological structure of the mountainous area, making it difficult to visualize structures using standard single-method geophysical approaches. Acquiring data of appropriate quality is an additional problem due to the complicated terrain, which often prevents sufficiently dense data acquisition [15]. Land cover (especially vegetation) or surface features of a landslide, among others, conditioned by geomorphological factors, can also strongly influence the results of remote sensing (RS) methods [13], which by their nature are suitable for monitoring the surface effects of subsurface changes. To accurately identify and interpret the landslide zone, a more integrated concept of data interpretation and state-of-the-art geophysical and RS methods are highly recommended [16,17]. Using this particular case study in Cisiec, we would like to evaluate the usefulness of integrated geophysical and remote sensing methods.

Many studies on landslides in mountainous areas show a broad approach to the topic. Ground-based, aerial, and spaceborne remote sensing systems are widely used to assess and monitor mass movements [18,19]. Systems enabling the use of free, high-resolution satellite imagery have been under development for several decades [19]. Satellite RS methods are particularly useful in monitoring sites in hard-to-reach mountainous terrain [20]. Earth observation imagery is applied to determine landslide susceptibility, detect mass movements, or identify phases of increasing landslide activity [20–23], as well as landslide inventory [24,25]. Grima et al. (2020) [26] used a geographic database of landslide events and land cover maps to describe the difference in frequency of these processes in forested and non-forested areas. They also determined the costs and benefits of forest protection or afforestation of landslide-prone regions compared to restoration in the Colombian Andes. Strozzi et al. (2018) [27], who described landslides from the Cordilleras of Peru, conducted studies using satellite synthetic aperture radar (SAR). SAR interferometry can also be used to monitor and evaluate landslide dynamics from a temporal and spatial perspective [28–30]. With the increasing popularity of unmanned aerial vehicles, optical and radar imaging of landslide areas is developing rapidly [18,31]. The digital aerial photogrammetry is widely used in studies of mass movements in the Carpathians [32–36]. The great potential of airborne laser scanning (ALS) in surveying inventoried landslides is also indicated [37].

Concurrently, terrestrial techniques are being developed intensively, which can be independent methods of data acquisition or complementary to other techniques, e.g., in case of difficulties related to landslide slope orientation and resolution of space-based data, or higher costs and/or difficult flight conditions for airborne data acquisition [19,38]. Among the key categories are terrestrial laser scanning (TLS), terrestrial optical photogrammetry, and ground-based SAR interferometry [39–41]. In recent years, the increase in the application of TLS, which enables rapid and dense sampling, is noticeable in the study of small landslides [42,43]. Wang et al. 2013 [42] determined the boundaries of an active landslide in a mountainous area of Puerto Rico's rainforest using a combination of airborne and ground-based LIDAR data, while indicating greater density as well as accuracy of the data by integrating ALS and TLS methods. Regardless of the proposed integration of RS methods, the effective application of TLS in landslide terrain depends on the surface's ability to reflect the laser beam, appropriate weather conditions, and the availability of reference points [44].

Geophysical methods support the interpretation and correlation of subsurface data with surface images [31]. Seismic [15,45–48], electrical and electromagnetic geophysical methods [32,49–54], or a combination of these techniques [55–58] have been applied in the study of sliding geological structures. Bruno and Marillier (2000) [45] conducted a differentiated geophysical survey on the Boup landslide in the western Swiss Alps and found that the techniques used can effectively investigate other landslides, but their application depends on the location. In many cases, geophysical methods have been used to identify landslide zones, landslide's lateral limit, and to describe the physical properties of mass movements [7,32,55,59–66]. Landslide movement is also a concern for ongoing monitoring using geophysical methods [67]. The combination of geophysical methods such as electrical resistivity tomography (ERT), multichannel analysis of the surface waves (MASW), and seismic tomography (SRT) can provide detailed information on the geological structure, landslide geometry, and hydrological characteristics. The compilation of different geophysical methods enables validation and verification of the reliability of the results [68]. The non-invasive methods are relatively effective and inexpensive [1]; however, they need the data to be mathematically inverted, which may be difficult and prone to subjective overinterpretation. Additionally, each geophysical method has specific limitations. ERT method is prone to water saturation, salinity, and porosity of rock matrices [69,70]. Moreover, high resistivity of the nearest surface layers can isolate the deeper parts from electrical current. Seismic refraction methods have a poor resolution in terms of reconstruction of vertical shapes of geological structures as well as detecting of low-velocity layers [71]. On the other hand, the MASW technique has poor result uncertainty which quickly increases with depth [72]. As a solution to each technique limitation, a multimethod approach was proposed in which data from each technique are supported by other method results.

Simultaneously, RS techniques are playing an increasingly prominent role in landslide detection and monitoring, as well as landslide susceptibility modeling [73] as methods delivering direct proof of subsurface changes visible on the surface. To monitor landslide processes, subsurface data obtained by geophysical methods are becoming more frequently supported by results obtained from multiple RS techniques, including the digital terrain model (DTM), providing precise data on the terrain's morphology [39,74]. Bichler et al. (2004) [56], investigating a landslide in Quesnel Forks in British Columbia (Canada), relied on geomorphological observations, including DTMs, to aid in interpreting geophysical data from ground penetrating radar (GPR), direct current (DC) resistivity, and seismic reflection and refraction surveys. Kamiński et al. (2021) [32] used multi-temporal DTM to estimate landslide kinematics and electrical resistivity tomography (ERT) to derive data on landslide structure and the tectonics of the flysch bedrock. Lapenna et al. (2009) [75] applied high-resolution DTM support by ERT for a detailed reconstruction of the Bosco Piccolo landslide in Basilicata region (southern Italy). Travelletti et al. (2010) [15] proposed a new approach for interpreting seismic refraction and reflection data on landslides by incorporating basic geomorphic information based on the sloping local base level concept, using data provided by the digital elevation model (DEM). Travelletti and Malet (2012) [76] also presented the integration of data from multiple measurement techniques (kinematic, geological, geotechnical, and especially geomorphologic—field observation, aerial orthophotography, DEM and petro-physical—ERT) in the form of a 3D geometric model of the Super-Sauze mudslide (Alpes-de-Haute-Provence, France) using geostatistical tools.

Given the complexity of mass movements, providing an integrated methodology for their characterization is a challenge. For this reason, a more comprehensive view of the landslide phenomena was presented in this paper. The main aim of the article was to propose an approach integrating the results of ERT, MASW, and SRT using synthetic modeling and uncertainty analyses. This allowed the spatial variability and slip area of the actively developing Cisiec landslide to be described and compared with previous studies. Apart from seismic and ERT methods, a terrestrial laser scanning-based DTM was created

by providing a detailed view of the landslide surface to interpret and correlate surface data with subsurface images.

The study area is located in southern Poland, in the Beskid Mountains within the Outer Western Carpathians. Area monitoring on the Cisiec landslide has been carried out since 2018. Detailed information about the landslide structure was needed to ensure the stability of the current structures because the study site is used as a ski slope. It is crucial for the safety of residents and skiers [65]. Due to the steep slopes and often lack of afforestation, these areas are very often modified to meet the demands of modern ski infrastructure [77]. At the same time, due to climate change, current winters are warmer and shorter compared to the same seasons occurring in the 20th century [78,79]. In order to extend the winter season and even ensure the operation of ski slopes, heavier artificial snow is produced and spread on the pistes. Because of the construction works disturbing the stability of slopes, added stress on the slopes, and after the winter–spring thaw, terrain once described as stable begins to move. This effect is so problematic that it has been briefly discussed [80].

The impact of anthropogenic factors [4,81,82] and relation between landslides and climate changes [2,83–85] were also noticed and described in multiple articles. Such complicated human–climate relation, as well as the impact of multiple additional triggering factors, is not fully studied and comprehended. However, by measuring changes in multiple subsurface physical parameters (seismic waves velocity, ground resistivity, magnetic parameters), it is possible to study and compare those uniquely triggered landslides.

The authors combined geophysical methods using synthetic forward modeling, limiting the possible interpretation errors and processed the data, cross-correlating results as proposed by Marciniak et al. (2019) [86]. By integrating the results of these methods in their uncertainty range through synthetic modeling, interpretation problems were resolved more quickly and a more accurate and complete image of the landslide structure was obtained.

The proposed methodology can effectively solve complicated seismic wave propagation problems and thus potentially allow for recognition of the nearest surface by using the most modern methods of full waveform inversion (FWI) and high-resolution reflection imaging (HRI). Because of the more precise initial model, it is possible to speed up data computation or even apply this method under challenging scenarios. The proposed approach was used in a landslide, where previous studies were conducted for a time-lapse comparison of soil movement evolution. In the present study, the relatively small surface changes recorded by TLS and information on subsurface structures resulting from geophysical surveys allowed a more complete estimation of the landslide development. The key novelty presented in this work is the concept of estimating the uncertainty of the results, which is essential for comparing the latest data, with information from previous studies. In addition, due to the correlation of different geophysical methods with each other and RS data, a synthetic verification of the presented approach and its effectiveness is vital. With additional terrestrial data, the present result is a unique example of a synthetically verified geophysical result, with precise surface time-lapse models. Such a concept can be beneficial for the utilization of the data in further studies, where time-lapse reflection imaging or geomechanically modeling of the landslide will benefit from precise and verified data. Moreover, the presented case study is one of the infrequent examples of recent geophysical studies in this landslide-prone region, where anthropogenic impacts are an additional trigger for landslide movements. Even though each case study is different, and it is hard to propose a general solution for all landslide studies, the proposed approach with necessary modifications can be applied in the detailed study of the landslides.

2. Materials and Methods

2.1. Study Area

Cisiec is located in southern Poland, Silesian voivodeship, in the Beskidy Mountains, Carpathians. The landslide is located on the northeast slope below Czerwieńska Grapa mountain (Figure 1a,b).

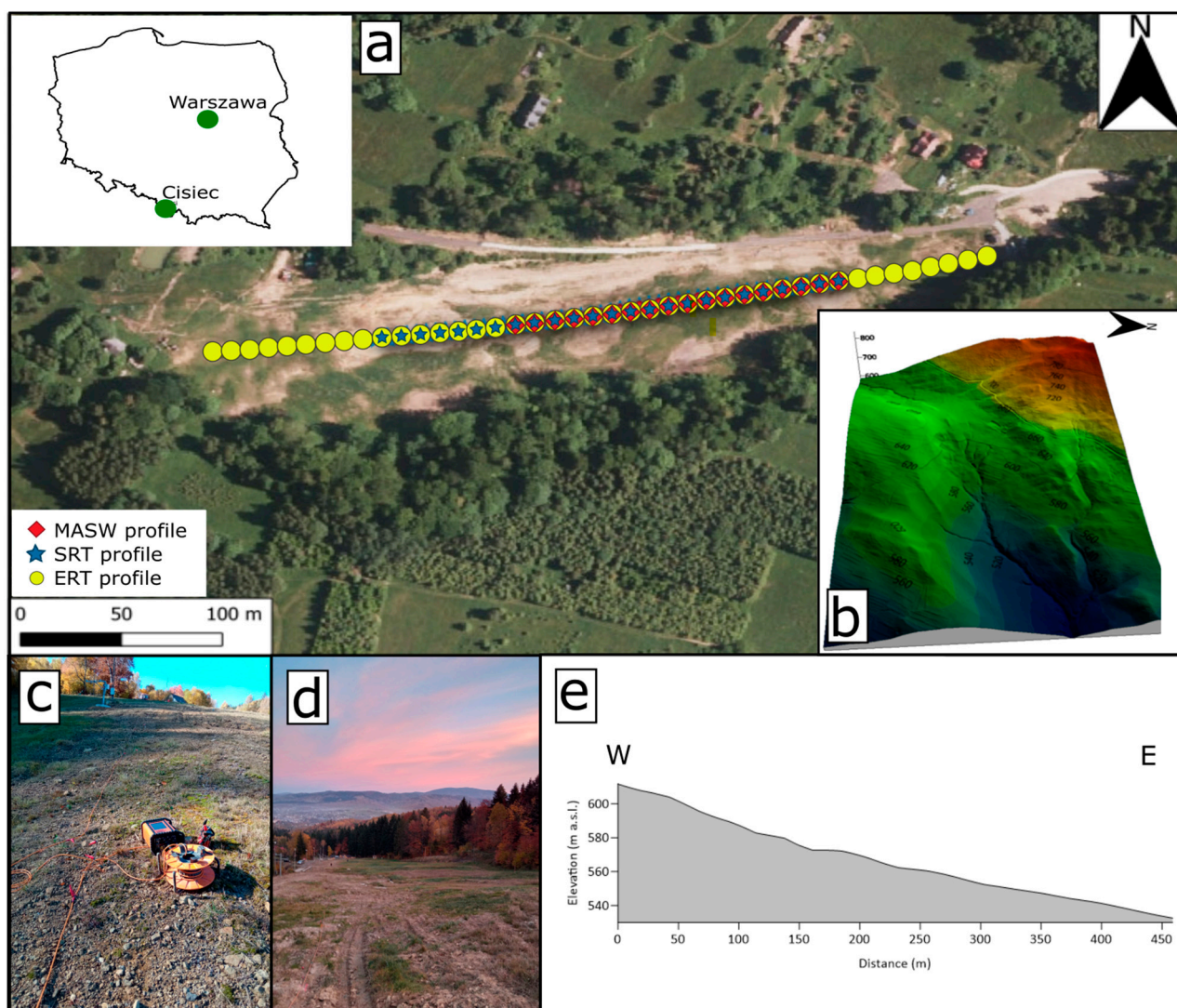


Figure 1. Overview of the study area: (a) Aerial photography of the Cisiec landslide from an OSM database with profiles of three geophysical methods [87]; (b) 3D model of the surface; view of the study area upward (c) and downward (d). (e) The elevation profile across the acquisition line.

The active landslide is located on the clearing surrounded by a forest and covers the meadow's central part (Figure 1c,d). The direction of movement is east–northeast and the height difference in the study area is about 100 m (Figure 1e). A watercourse along the slope from N and S sides and subsurface flows are present. The study area is located in the Outer West Carpathians, Silesian Nappe unit (Figure 2), with two tectonic elements: bottom—Cieszyn unit and upper—Godul unit [88]. The study area is situated on the hieroglyphic beds and variegated shales. The hieroglyphic beds are an example of Carpathian flysch and consist of thin-bedded or medium-bedded fine-grained sandstones with numerous organic hieroglyphs and gray, black, and dark green shales (Figure 3). Their age is the middle and late Eocene when sedimentation was calm [89,90]. The age of variegated shales is the same. These lithostratigraphic units overlap with each other and appear above and below each other [91]. The hieroglyphic beds lie on the Cieżkowice sandstones or variegated shales and under menilite beds. Variegated shales lie on the Istebna beds and under hieroglyphic beds or menilite beds. The thickness of the whole unit may reach up to 200 m [91]. The geological structure shown contributes to the increased susceptibility to mass movements [63].

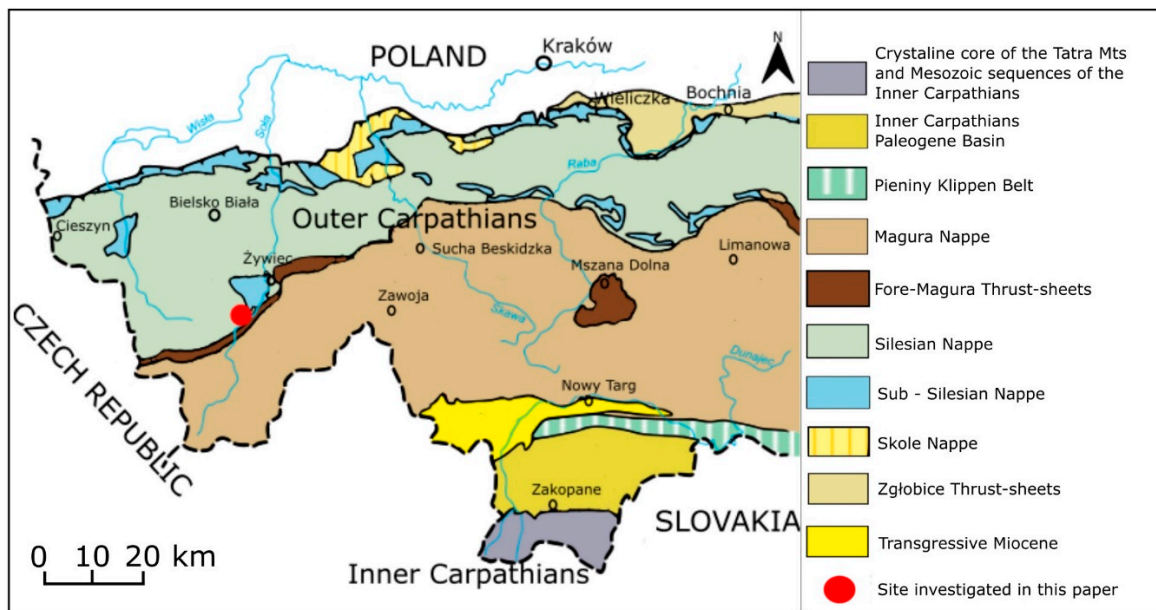


Figure 2. Tectonic map of the Outer Western Carpathians in Poland (after Cieszkowski et al., 2006 [92]; modified) with the location of the research investigated—the red dot.

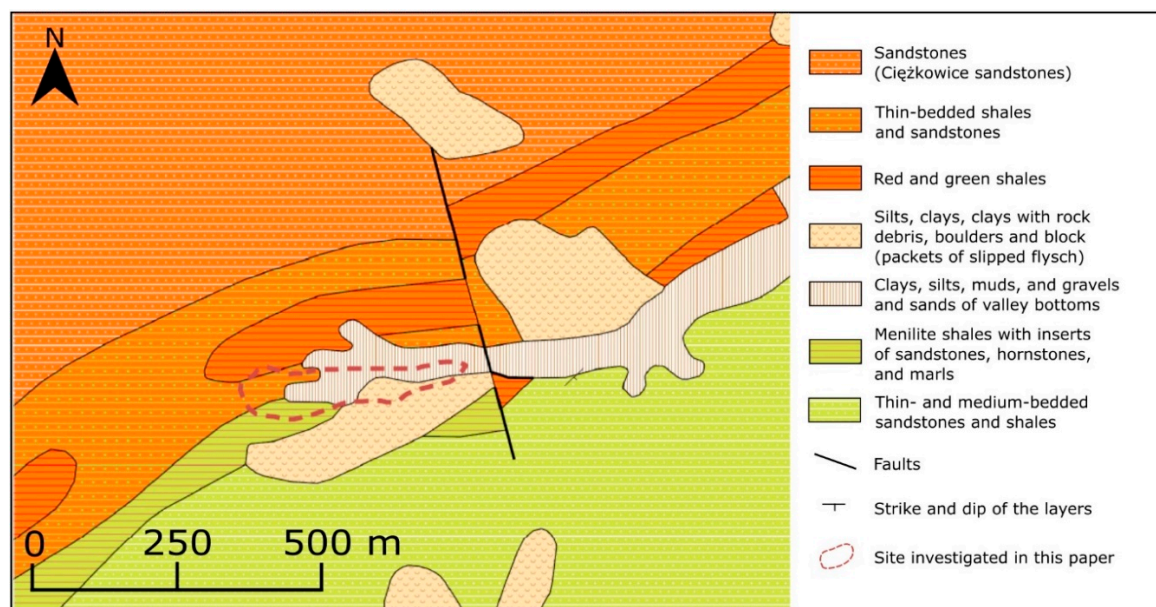


Figure 3. Geological map of the study area (after PGI-NRI [93]; modified).

2.2. Fieldworks

According to the result of previous studies, of similar landslides in the region [63,66,94–96] and the Cisiec landslide [65], the multimethod approach integrating ERT, seismic refraction, and TLS was chosen to be optimal to measure relative evolution of the sliding structure. Because the geological construction of the study site has multiple almost vertically oriented structures, as well as a strongly contrasting geological composition of shales and sandstones, the proposed approach seemed to be optimal in solving expected imaging limitations.

ERT and seismic measurements were conducted across a common profile line. The data were gathered in October 2019. The profile line was in the middle of the ski slope (Figure 1a) and was designated using the Leica Viva GPS Real Time Kinematics (RTK) system [97]. The ERT profile was 400 m. The distance between the electrodes was 5 m.

Measurements were made with the gradient array. This arrangement of electrodes and this layout allowed surveys to be carried out to a depth of 80 m. The 81 electrodes were connected to the resistivity meter ABEM Terrameter LS [98]. The SRT was performed using an ABEM Terraloc recorder [99] with 48 10 Hz geophones spaced every 5 m. The 10 Hz geophones were chosen to be optimal for common data gathering for both refraction and surface waves surveys, as they do not limit MASW recognition range without adding additional strong low-frequency noise to the refraction data. The total profile length was 235 m. The excitation of the seismic signal was carried out with an 8 kg sledgehammer and a metal plate every 5 m. Three signal excitations were vertically stacked at every shoot point to obtain better data quality. The MASW profile begins at 70 m of the seismic profile and has a total length of 165 m.

TLS was performed in 2019 in May and October. Such periods were chosen to visualize the slope surface in the different soil moisture states. The May investigation showed the maximum soil moisture after winter for later comparison of changes due to dominant snow-load. The October measurements visualized the state after summer, where the rock structures were less water saturated. The RIEGL VZ 6000 [100] relocated across four points to cover the whole sliding zone was used for precise measurements. Each scan was done using the effective measurement rate equal to 222,000 meas/s with an accuracy of 15 mm and precision of 10 mm. The position of each TLS measurement point was measured using the Leica Viva GPS RTK system connected to the GNSS reference ASG-EUPOS station [101] located in Żywiec (Poland). This allowed positioning errors to be reduced to less than 10 cm for each direction. The used configuration allowed for the creation of dense DTM models, with a resolution not worse than 0.1 m and a good correlation between the two datasets.

2.3. Data Processing

The data processing was divided into three key steps to recognize the sliding structure (Table 1)

Table 1. Data interpretation steps.

Step	Step Name	Target	Outcome
1	Simultaneous geophysical data processing	Recognition of the subsurface structures with information cross-correlation between methods	Geophysical images of the subsurface
2	Digital terrain model construction	Construction of the aerial surface model from two TLS datasets	Recognition of the changes visible on the surface
3	Data integration and uncertainty estimation	Synthetic verification of geophysical data to estimate result uncertainty, integration of aerial and subsurface data to final model creation	The final subsurface model with information about changes occurring during May and October 2019. Information about the uniformity of the sliding structure by comparison of data from previous studies with the latest data

2.3.1. Electrical Resistivity Tomography

The Res2DInv program was used to process and interpret resistivity data [102]. Before data processing, a topography was added from the prepared GPS data. The robust L1 norm standard with parameters set by default by the program was chosen (no extended model, normal model cells with the same widths of one unit interval (5 m) and the finite-element method with trapezoidal elements). The robust inversion method was used with a cut-off factor constraint of 0.05. Calculations were made using robust constraints and the Gauss–Newton method for calculating the Jacobian matrix. The number of measured data was 1072 points, and the number of inverted data was 1066 points. The number of iterations was 5. The root means error RMS was 2%.

2.3.2. Multi-Channel Analysis of Surface Waves

The MASW method allows V_s velocities to be estimated in the shallowest part of the landslide (Figure 4). Because surface waves respond most effectively to changes in velocity in the nearest surface [103], they contributed to better interpreting the structure of the colluvium [104].

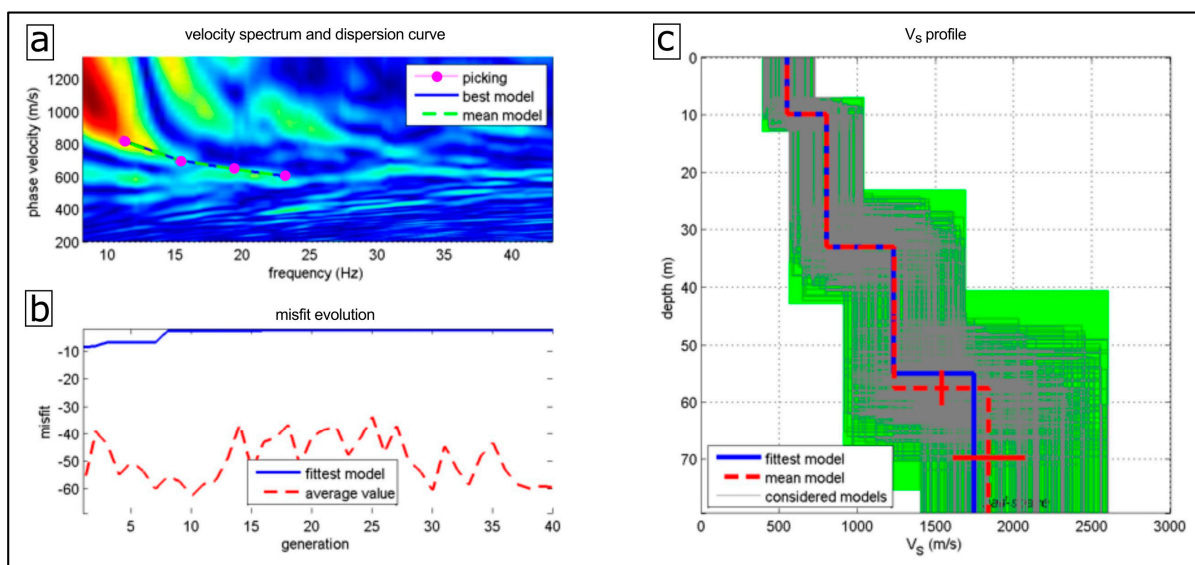


Figure 4. An example of the dispersion analysis (shot number 1037): (a) The velocity spectrum and dispersion curve with clearly visible main mode; (b) the misfit evaluation shows rapid inversion convergence; (c) considered models of S-waves profiles with the best and mean models show clear four layers structure.

The WinMASW program was used for data processing. To provide an optimal number of at least 12 geophones in each seismogram, as well as to maintain a shoot receiver offset of 5 m, 36 seismic recordings were selected. For each shot, gather dispersion curves were determined (Figure 4a), and depth profiles of changes in the S wave velocity were made, from which a 2D model of the profile was developed. The data processing started with 1D filtering, which eliminated signals lower than 5 and 50 Hz. Additionally, the first breaks of the refraction were cut from the recordings to eliminate additional bias during dispersion curve modeling. All procedures were done using industrial scale software Globe Claritas. After processing, the dispersion curve was visualized and picked. Only the fundamental mode was picked, due to the complicated behavior of surface waves across the profile. Such an approach was chosen as the most reliable in terms of uncertainty in cases, where higher modes cannot be certainly picked (Figure 4b). For the inversion, four layers with half-space at the bottom were determined. The velocities for each interval are presented in Figure 4c. For dispersion curve inversion, a genetic algorithm was used [105]. From a single seismogram, the 1D model was obtained. The 2D model was created from 36 1D models. The obtained results have relatively low uncertainty, not exceeding the 30 m/s average and 10 m/s for the best-fitted model.

2.3.3. Seismic Tomography

The seismic tomography was done using the Globe Claritas processing package. As a starting model, four layers were assumed based on the results of LVL (low-velocity layer) analysis of first breaks (Figures 5 and 6a). The first two layers have dense 5 m bin spacing in the horizontal direction. The deeper layers, where refraction analysis is less precise, have a 20 m bin size (Figure 6b). The initial model was based on approximations from initial LVL analysis, MASW data, and results of previous studies [65]. The picked first breaks from the dataset were QC (quality control) analyzed to eliminate cycle-skipped picks. The

thickness of each layer was determined for all shots, and a velocity model was created to obtain a 2D model (Figure 5). The layer stripping approach, where the uppermost layer is fitted and later fixed, during the fitting of the next, deeper layer was used. The inversion process took 50 iterations to obtain a good effect. As a result, the model with a low RMS of 1.27 ms was obtained.

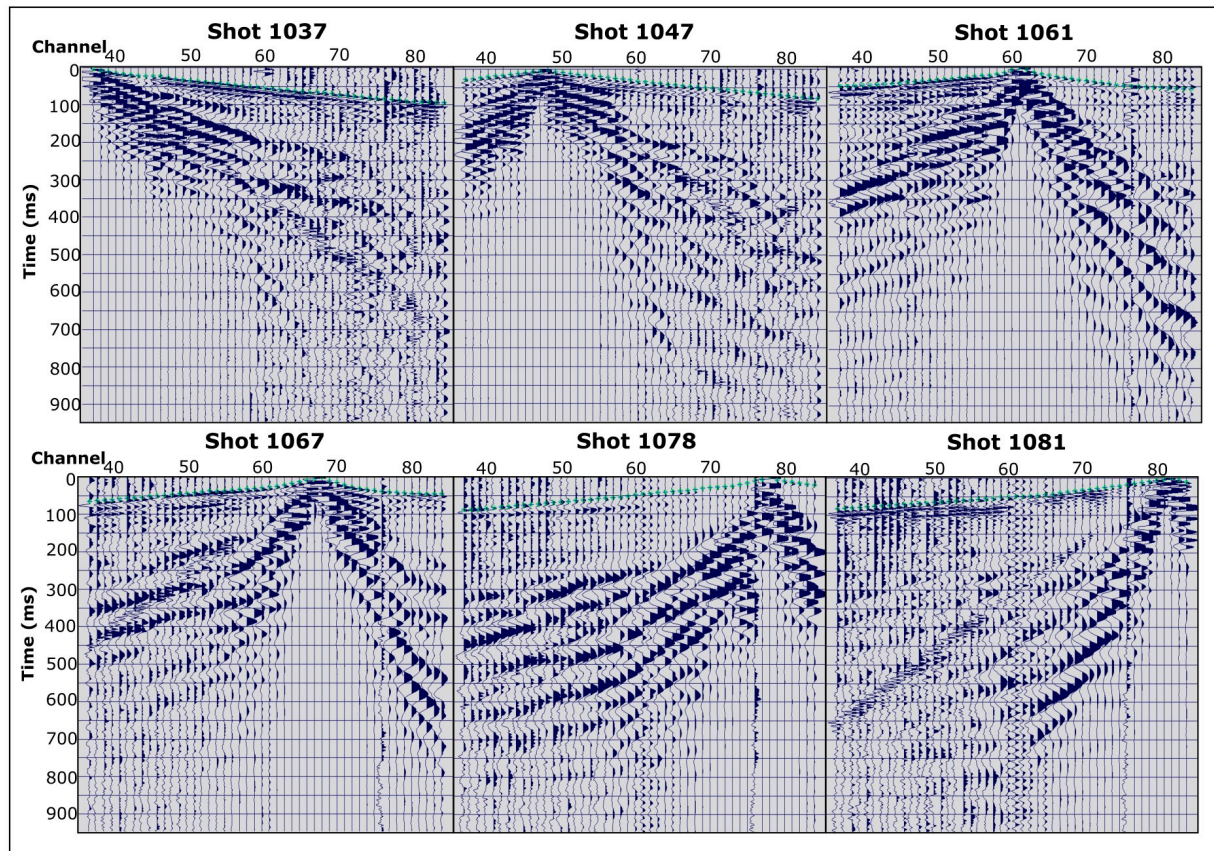


Figure 5. An example of a recorded shot gathers across the whole seismic line with marked times of the first breaks of the seismic wave. The strongest surface waves are visible up to 0.7 s.

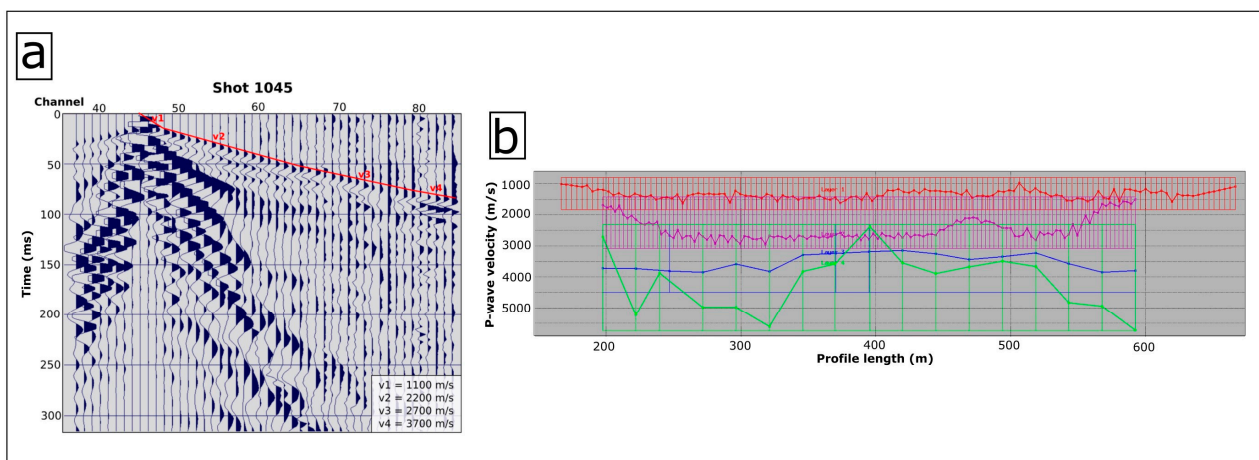


Figure 6. Seismic data processing: (a) The setting of four geological layers on the hodograph; (b) parameterization of the velocity field with a separate grid for each layer at the final step of the inversion. Solid lines show the boundaries in the structure.

2.3.4. Digital Terrain Model

Digital terrain models were created using data acquired from TLS. The point clouds were processed in RiSCAN PRO 2.11.3. Each object was assigned coordinates extracted from the Leica Viva RTK survey. A single scan was pre-filtered and points with a deviation ≥ 20 , and reflection ≤ -20 dB were removed. Isolated points for which there were fewer than 10 measurement points within a 5 m radius were also removed. The multi-station adjustment (MSA) tool was used to merge the separate point clouds. The next step was to remove vegetation and artificial objects using Terrain filters. The result was two separate 3D DTM clouds (May and Octree) with an MSA error (standard deviation) of less than 0.08 m. After Octree filtering, the 3D DTM clouds were exported to ASCII files as 2D DTM (X, Y, Z) data with a resolution of 0.10 m. The accuracy calculated from the root mean square error (RMSE) for May DTM was 0.22 m and for October DTM was 0.19 m. The data were saved in the ETRF2000-PL/CS2000/18 coordinate system. Comparison of the 2D DTMs was done using QGIS 3.26 version.

In order to maintain consistency in field measurements and post-processing, the same measurement methods and equipment were used each time, and the surveys and data processing were carried out by the same team. In this way, we achieved repeatability of measurements with as few errors as possible.

2.3.5. Data Integration and Synthetic Modeling

Data from ERT, SRT, and MASW were integrated to obtain more reliable results. To better recognize the surface structures of the landslide and its changes over time and to locate the individual survey points more precisely, RTK measurements and TLS were carried out. The linking element in the presented case is forward modeling for geophysical methods. The synthetic model is based on the information from SRT, ERT, and MASW data. Seismic tomographic methods provide smooth models, without information about the shapes of geological structures, similar to the MASW technique. However, both S-waves and first breaks of P waves are sensitive for those structures and can be reproduced using the FWI technique. One of the drawbacks of FWI is the reproduction of the nearest surface based on smoothed models which require additional computational effort. In the presented work, we used information from the ERT method to add structural shapes to tomographic results. Such an approach has two main goals. Firstly, it is to verify the result's uncertainty by comparison of P-wave velocities created by the integration of methods models with real data, and secondly, to simplify wavefield estimation of the nearest surface. The data are clustered by replacing the velocity V_p from SRT and V_s from MASW. Because of the low amount of data and shorter seismic line than the ERT profile, the manual assignment of resistivity to the velocities in certain ranges was done. However larger-scale experiments will require a machine-learning approach. To compare synthetic seismic data to real shot gathers, synthetic wavefields were calculated at positions corresponding to the "real" positions of shoot and receiver points in the model. Thus, the side parts of the synthetic model, where only ERT coverage was present, were used as an absorbing boundary to attenuate possible wave reflections from the model boundaries. Such an approach is necessary to obtain the modeled velocity field without numerical effects that can complicate the comparison of real and theoretical shots. A synthetic wavefield is generated using the software SOFI2D (seismic modeling with finite differences) [106]. This paralleled code is used for modeling based on finite differences (FD). Thanks to its use, the precise estimation of processing approximations was possible for better estimation of result uncertainty. With this approach, the propagation of seismic waves in the near-surface of a complicated environment can be reconstructed, then compared with real data, and checked if similar effects from geological structures can be identified. The obtained information can be treated as a more precise solution for estimating velocity fields on the nearest surface, with strong residual zones. In addition, the proposed approach made it possible to determine the impact of each of the information used on the final subsurface model based on the high-resolution DTM created.

3. Results

The ERT measurements allowed for the recognition of the rock structures up to 100 m depth (Figure 7a). In the bedrock, three resistivity complexes were distinguished. On the profile up to 160 m and at 250 m, just below the surface, there is a complex of shale and sandstones with a resistivity of 100–200 Ωm (Figure 7b). From 160 m of the profile is low resistivity anomalies (values 10–40 Ωm), interpreted as complex shale with sandstone with a significant amount of shale. This is landslide colluvium. Below are sandstones with a resistivity of 60–80 Ωm . The slip surface was determined at a depth of 30 m on sandstone formations. When determining the depth, it should be considered that with an electrode spacing of 5 m, the vertical resolution at depths 30 m is 5.1 m (Figure 7a).

Using the seismic refraction method, four layers were determined to be significantly different from each other in the P-wave velocity (V_p). The first layer (I) has an average thickness of 10 m and an average P-wave velocity of 1200 m/s (Figure 8a). The thickness of the second layer (II) is approximately 20 m and V_p velocity of 2300 m/s. The next layer (III) is 30 m thick and has an average V_p velocity of 3300 m/s. In the fourth layer (IV), average V_p velocity is 4500 m/s. From 150 m to 270 m in length of the profile, the slip surface of the landslide is visible. Different velocity values distinguish it in the third and fourth layers, as well as resistivity values. Such a situation indicates that slip occurs on contact between geological layers. The accuracy of P-wave velocity estimation for the first layer is ± 50 m/s and for the second and third layers is ± 100 m/s (Figure 8b).

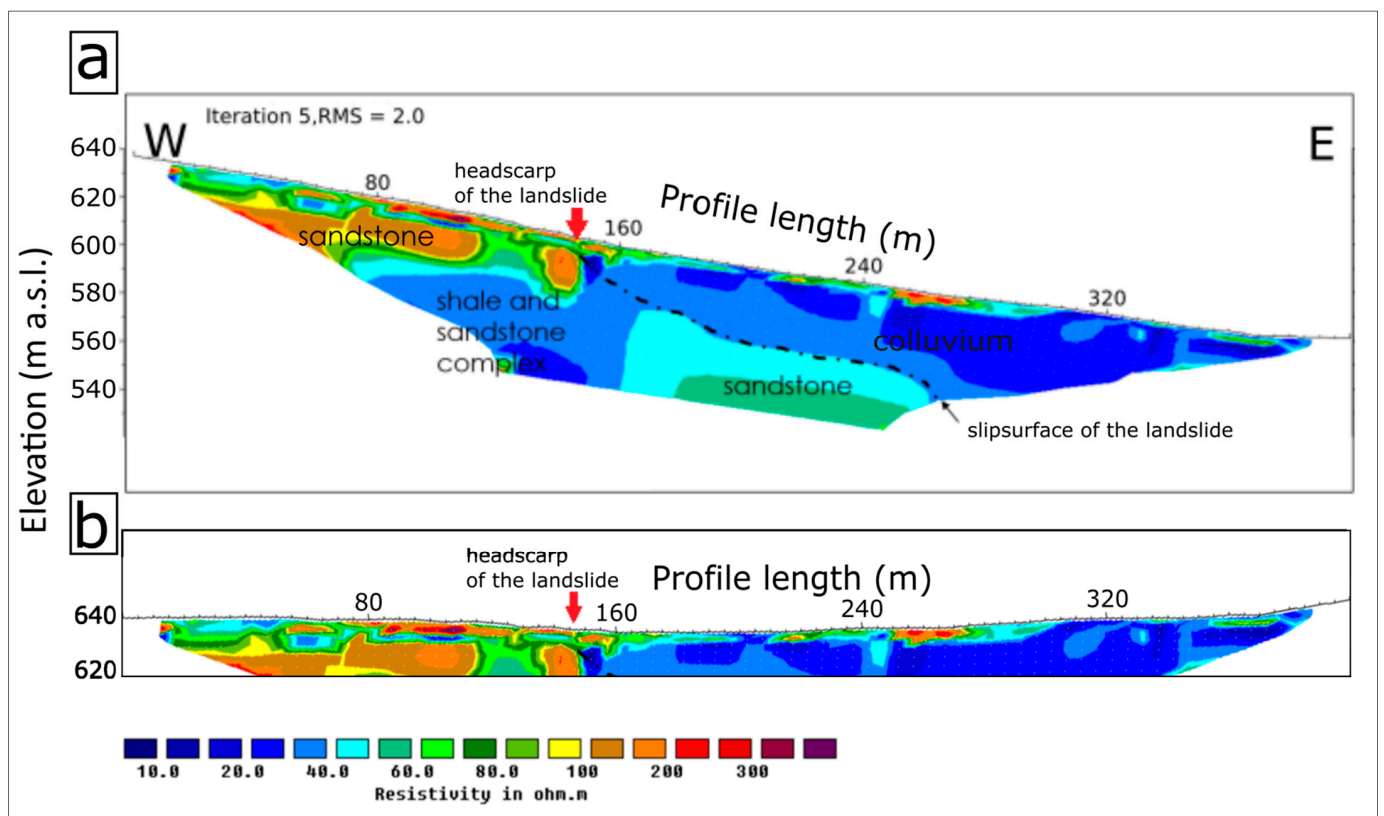


Figure 7. Inversion results of ERT measurements showing the slip surface (dashed line) and headscarp of the landslide (red arrow). In this profile, significant structural variations in the form of variable resistivity values are observed: (a) The whole measuring profile with actual height; (b) the first 20 m depth showing the complexity of the uppermost structure.

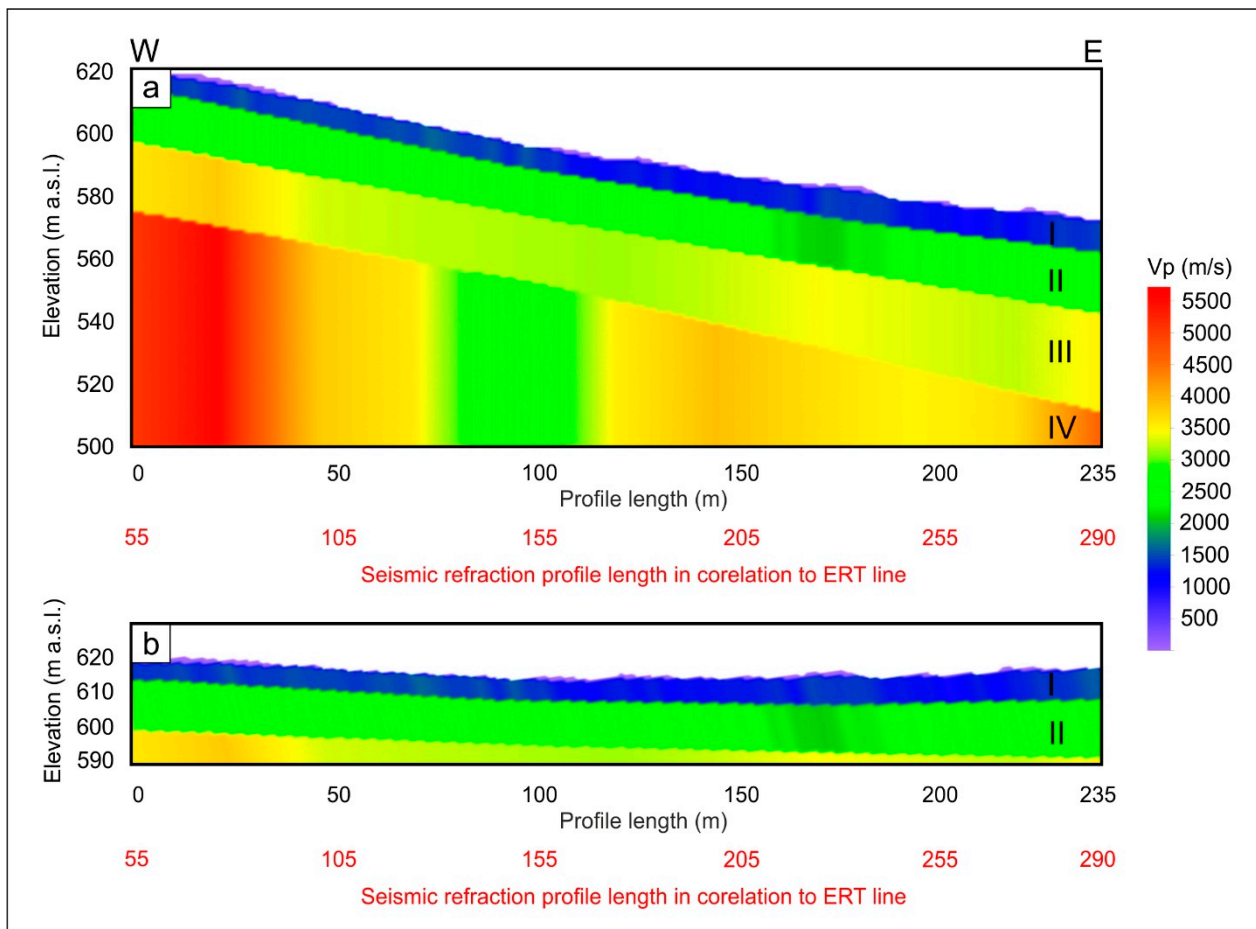


Figure 8. The seismic refraction tomography result shows a clear layered structure with significant horizontal and vertical variation of seismic velocities: (a) The whole profile; symbols of layers (I–IV) with matched average V_p velocities: I—1200 m/s, II—2300 m/s, III—3300 m/s, IV—4500 m/s; (b) zoom for depths of 0–30 m without elevation.

The beginning of the MASW profile is at 70 m of the seismic profile, and its total length is 165 m, as presented in Figure 9. In the analysis of surface waves using the MASW method, the search depth reached about 50 m. It was also possible to distinguish three layers. The first layer is about 7–12 m thick and has an S-wave velocity of 300 to 500 m/s. The second layer is approx. 15–20 m thickness and S-wave velocity of approx. 500–700 m/s, and in the third layer with a velocity above 1100 m/s. The accuracy of S-wave velocity estimation for the first layer is ± 100 m/s, for the second layer ± 200 m/s, and for the third layer ± 500 m/s.

The comparison of the DTMs from May and October made it possible to compare the image of the landslide surface (Figure 10a,b). There is a noticeable constant activity of the landslide (Figure 10c). The land slides in an eastward direction by about 1–3 m. The greatest activity is observed in the upper part and the lowest in the lower part of the landslide.

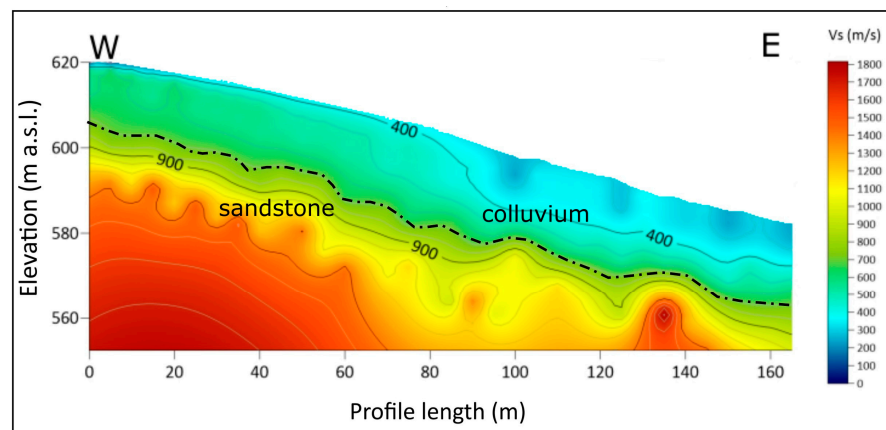


Figure 9. The MASW result. The slip surface is marked with a dashed line. At half the length of a profile, a clear change in S-wave velocity was observed. At the bottom of a profile, there is a structure with a higher seismic wave velocity interpreted as bedrock.

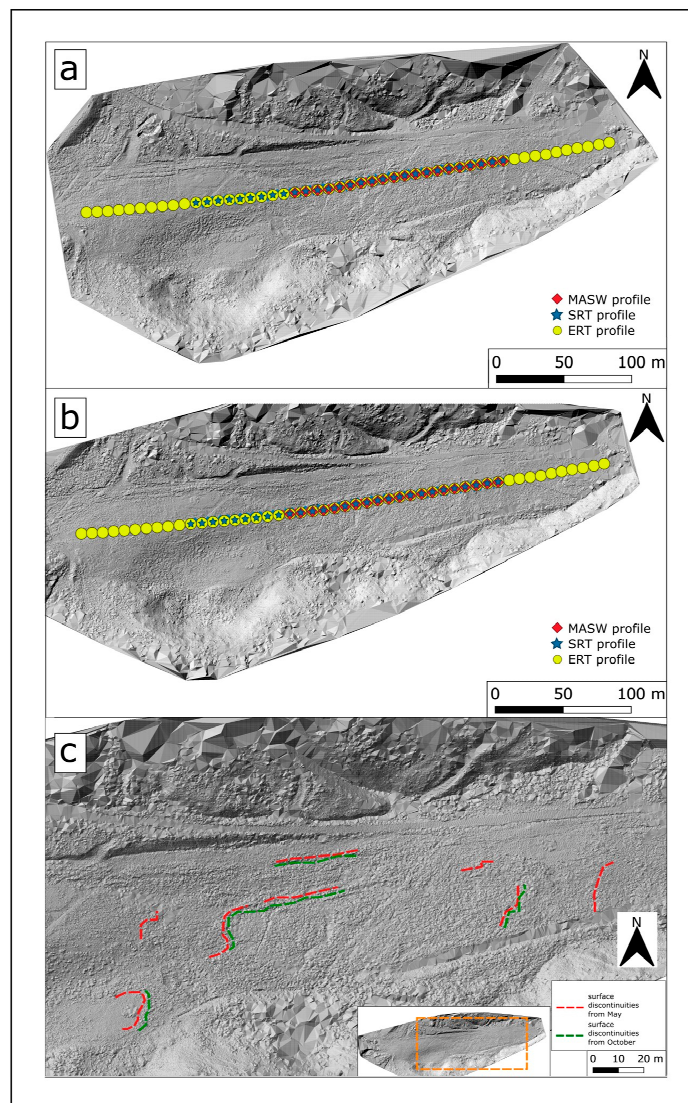


Figure 10. Graphics showing the variability of the landslide’s surface using the DTMs: (a) The model made in May 2019; (b) the model made in October 2019; (c) the model showing analysis of surface

displacements in the landslide. The displacement planes were identified by direct observation in the field, as well as a comparison of the DEM models.

4. Discussion

In most cases, the application of the standalone geophysical approach leads to simplified results, that can be misleading during interpretation without detailed surface data. Proposed in the article integration of multiple geophysical and remote sensing methods can provide significantly higher resolution and precise recognition of the landslide [31].

The proposed methodology integrates the ERT measurements with MASW and SRT in terms of subsurface methods. The joining element in the presented case is forward modeling. Because of the sensitivity of MASW and electric methods to water content in rock formations, such methods are well-suited for landslide investigations. However, the main drawback, which is limited resolution in the MASW case, and lack of precise result verification in terms of ERT, have a significant impact on the final interpretation and possible misleading conclusions. The synthetic verification of the results can solve described problems as a solution. By building the synthetic model based on the information about structure shapes from ERT, V_s velocity from MASW and V_p velocity from SRT, we could generate synthetic seismic shot gathers and compare them with real data. The data comparison allows for the estimation of similar effects from geological structures. Additionally, the proposed approach allowed for estimating how strongly each piece of information from a single method influences the final subsurface model. The proposed approach is cost-effective and provides spatial information, which is not possible with borehole data. Because the acquisition is one of the most expensive parts of similar case studies, the proposed methodology based on the same seismic dataset does not raise the overall cost. The additional computational effort, despite being on average two times larger, is still beneficial in the overall increase of final result reliability. Moreover, near-surface processing is relatively fast. The proposed approach is only slightly more expensive than a single method or multiple methods but done separately.

The proposed approach allows for solving multiple processing and interpretation problems:

- Recognition of complicated geological structures in a mountain environment
- Distinguishing between the geological construction of the study site and the landforms created by soil movement such as faults, the surface of rupture, sliding bodies
- Estimation of the uncertainty of the results by the use of information about each result's reliability during synthetic model building
- Cross-correlation of the information from different methods
- Final result integration and validation by integration of data from electric and seismic methods, and it is verified by comparing real seismic records with those obtained from synthetic data
- The problem of seismic wave propagation on the nearest surface is crucial for utilizing FWI and reflection imaging techniques.

Due to the correlation of the data and subsequent clustering, more geological structures can be distinguished (Figure 11). In the P-wave, there is a geological structure with a velocity of approximately 2350 m/s, in S-wave velocity of approximately 300 m/s. In this place, the geological structure is probably more waterlogged, which is also seen on the ERT, where it manifests itself with very low resistivity.

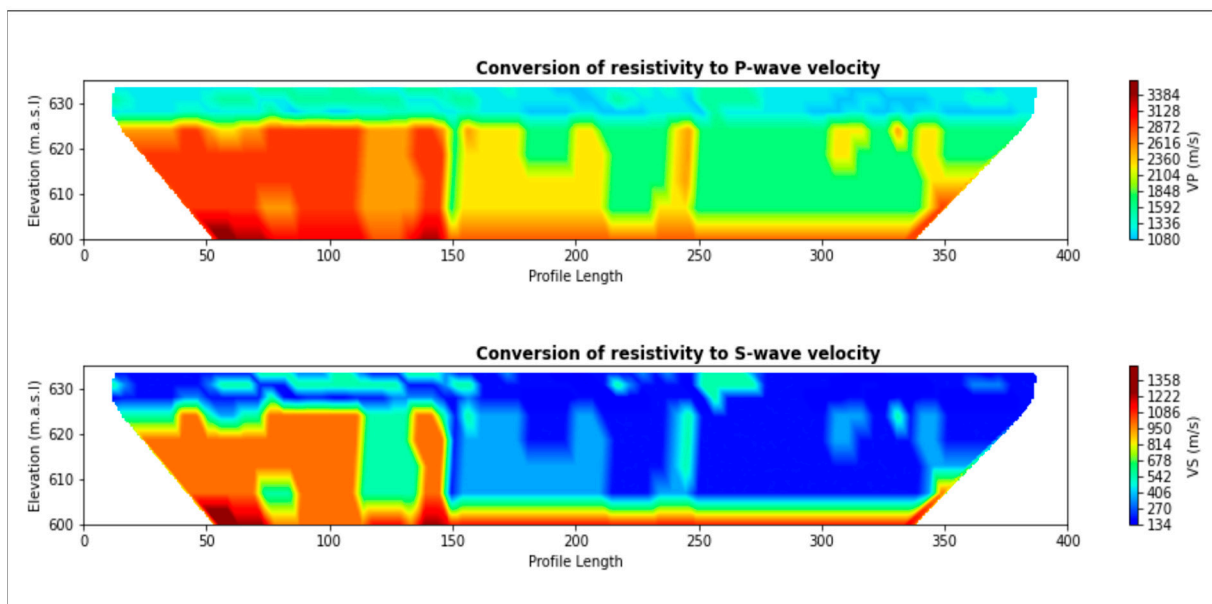


Figure 11. The synthetic models based on the integration of ERT, SRT, and MASW data. The assignment of the velocity to the resistivity values was done manually, in margins as tight as possible. Such an approach allowed for the solution of a problem with different profile lengths, because of the clusterization of values to specific rock types. As a result, most of the structural information from the ERT method was preserved.

The accuracy analysis performed takes into account the error of the technique. For seismic, RMS is 1.47%. Comparing the synthetic model with the real model (Figure 12) using the times of the first waveforms, it can be seen that the models agree. The same system of layers is present. The velocities in subsequent layers differ from each other by ± 100 m/s, which is within the limits of the determined error. Due to acoustic approximation, the S wavefield cannot be correctly reproduced, and thus requires a fully elastic approach. It is visible on the generated Love waves. Table 2 shows that the matching error is small. In the first layer, the difference in velocity is the smallest.

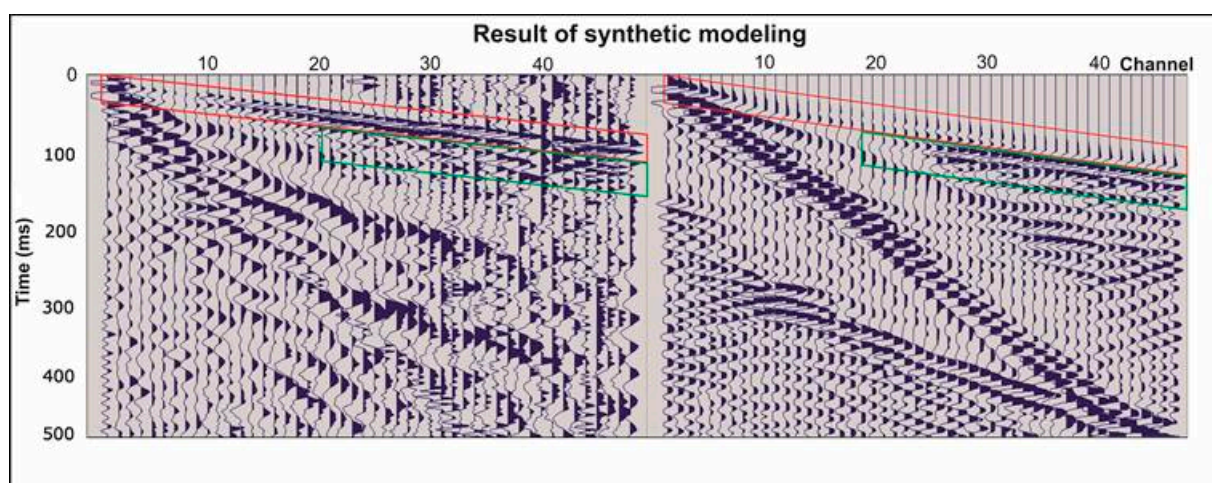


Figure 12. Comparison of the field observations (left shot gather) with the synthetic model wavefield (right shot gather). The main characteristics of the wavefield can be recognized and compared, including refraction (red frames), and reflections (green frames).

Table 2. The first P-waves velocity in real and synthetic models.

Layer	Velocity in the Real Model (m/s)	Velocity in the Synthetic Model (m/s)	Difference (m/s)	Difference (%)
1	1110	1120	10	1
2	2640	2610	30	1
3	2960	3030	70	2
4	4730	3550	1180	25

The deeper the layers, the more error-prone the seismic data and their interpretation. The error of the method influenced the difference in the velocity of wave propagation in individual layers, the accuracy of the approximation, the exact density value unknown, and the rock material sliding, which disturbed the original structure of the medium and changed its physical properties.

One of the most important problems of landslide research is to identify the depth, course, and shape of the slide surface [5]. The final interpretation model (Figure 13) allows for distinguishing slip surfaces, with several structures in the sliding body. The overall shape of the landslide colluvium was imaged. Additionally, rock structures formed from shales and sandstones can be distinguished. The image reveals a relatively large dip in rock structures. Moreover, the overall information from ERT, MASW, and SRT data indicates that the study site is characterized by relatively high velocities of non-sliding rocks, whereas resistivity values can be described as low across the whole line. The V_s values estimated from MASW data indicate low soil compactness in the sliding part. It is worth noting that V_p velocities are significantly higher than V_s values, especially for deeper layers. It can be interpreted as strong velocity anisotropy; however, such phenomena require further studies. At this stage of the survey, the hypothesis that at the deeper layers, we can observe fractured rock structures just below the surface of rupture can be stated. The correlation of geophysical data with the DEM model reveals that the sliding body is rather uniform in movement (Figure 13). Despite the low compactness of the sliding body, the whole landslide has similar displacements on all visible faults and surfaces of rupture. Because the displacement was estimated for the spring–autumn period with the first remote sensing measurements shortly after winter, it can be stated that changes in soil moisture, as well as a mass of artificial snow and its thawing, are the main triggering factor to this landslide. Compared to the previous study in this landslide [65], we can observe almost identical velocities of V_p between data from 2018 and 2019. This indicates that precisely measured from TLS methods in this work, slip is caused by seasonal hydrological changes, additionally amplified by anthropogenic actions. Moreover, it also indicates that the whole initial structure of the sliding body is preserved, despite the occurring movement.

Using the analysis of changes in the velocity of the longitudinal wave V_p , the geometry of selected landslides in the Polish part of the Carpathian Mountains was also estimated [63,66,94–96]. Studies of the nearby Milówka landslide have revealed the presence of two slip surfaces that correlate with refraction boundaries [63]. In this case, the ERT result reveals the shape of the slip surfaces. The estimated maximum thickness of the landslide in Cisiec is 36 m, while in other areas of the Polish part of the Outer Carpathians colluvium thicknesses of 30 m have also been recognized [66,96] based on the electrical-resistivity method.

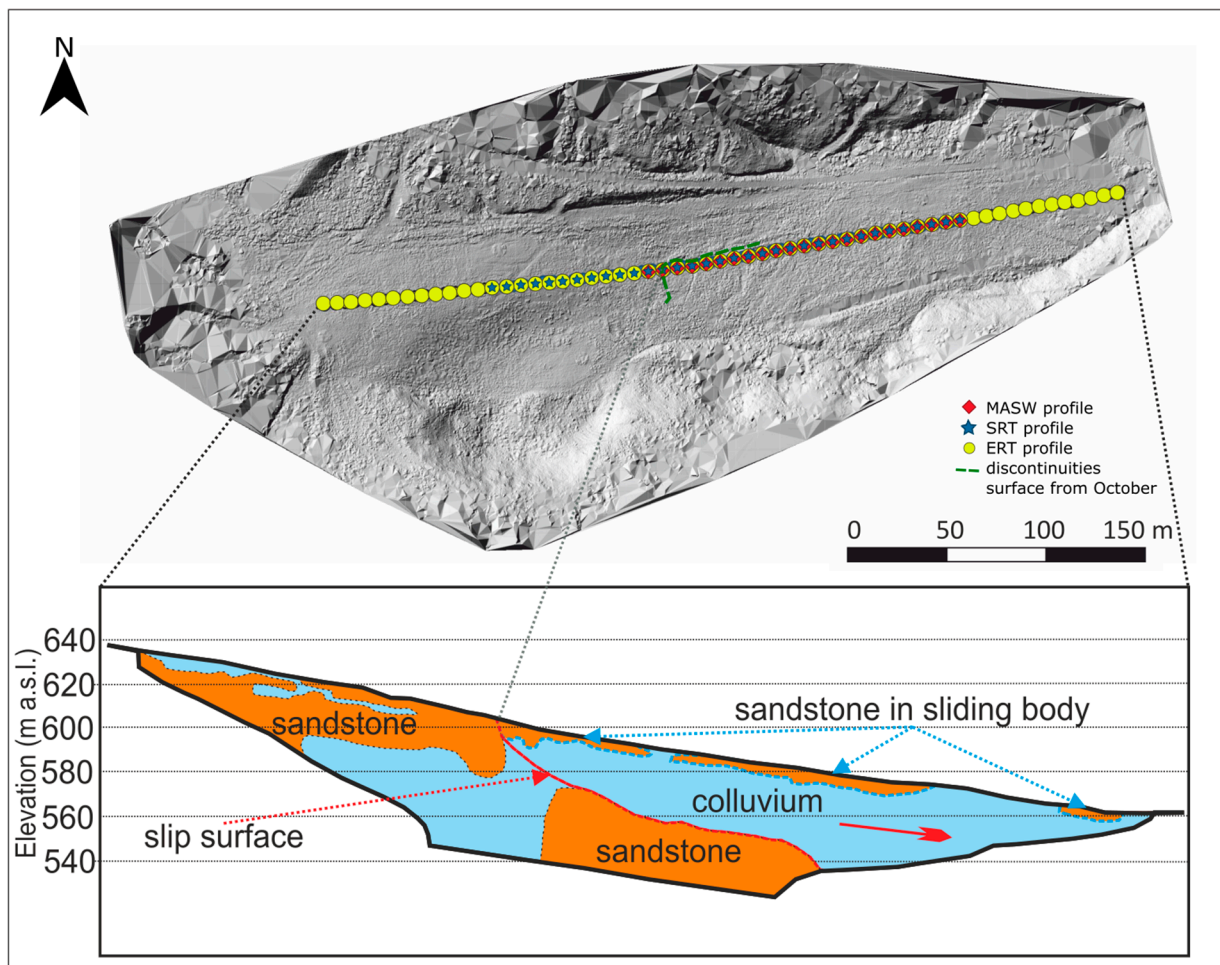


Figure 13. Interpretive image based on the obtained results in correlation with the DEM. The red arrow indicates the direction of the landslide movement. The integration of remote sensing and geophysical data allowed for the recognition of the landslide headscarp, and the estimation of colluvium displacement in time.

Since the presented results illustrate a landslide where human influence in the form of artificial snowmaking on the slope is an important factor, it can be noted that the landslide itself, despite the movement, is quite homogeneous. The reason for this can be attributed to the stiffening effect of the highly compressed and firm-transformed artificial snow layer, which causes homogeneous pressure on the landslide plane. In addition, the freezing effect of thick snow cover seasonally “binds” the landslide body, causing the soil to remain homogeneous even in spring, where the thawing effect is thus more uniform. A similar effect was described in the work of de Jong et al. (2014) [107], where a significant increase in ground compaction and thus variability in ground permeability was observed. This explains the greater susceptibility of ski slopes to surface erosion, also observed on the landslide in Cisiec. The additional influence of snow cover has been extensively discussed by Matsuura et al. (2014) [108] and Kawagoe et al. 2009 [109], where, in Japan, natural heavy snowfall has a significant effect on changes in hydrological properties, including fluctuations in water pressure in the geological medium, and is thus closely related to landslide movement.

As stated in the introduction, one of the purposes of this paper was connecting ERT, SRT, and MASW methods using synthetic modeling and uncertainty analyses to check the spatial variability and the slip surface of the Cisiec landslide. The idea of a multi-geophysical methods approach, which can be adapted to diversified case studies, was noted several decades ago [45,56]. Despite the fact that each landslide is unique,

a general concept utilizing multiple geophysical techniques was proposed by several researchers [45,47,55,56,110], however without in-depth uncertainty analysis. Following the necessary modifications to the acquisition parameters, as well as to the data processing and interpretation steps, the proposed approach in the article can be easy to adapt to other cases. Thanks to the combination of multiple methods and their correlation, taking into account measurement errors and making a synthetic model, it was possible to recognize the geological structure more accurately—this concept minimized the ambiguity of the interpretation of geophysical measurements. To reduce interpretation inaccuracy, the best way would be geological drilling. However, verifying the result with drill cores is more expensive, and data provides only point information. In the future, the methodology presented in the article will be used for the long-term, time-lapse observation of the described study site. This will allow for the analysis of changes over time and the evaluation of possible anthropogenic triggering of the landslide.

5. Conclusions

The proposed methodology of integrated geophysical surveys with synthetic verification consisting of resistivity and seismic measurements can be used to precisely determine the shallow geological structure of a landslide in geologically and tectonically complex regions. This concept also helps in determining the times of the seismic arrivals in the datasets for different wave types. Such an approach can be integrated with modern methods, such as FWI and HRI, in further studies. These methods, providing much more accurate and detailed resolution of subsurface images, require well-described initial models, and multiple a priori information to be effectively applied to near-surface studies. Among these data are precise velocity fields with well-constrained geological structures, which can be further enhanced with details from these methods. Additional boundary conditions will reduce computation time by constraining the solution space. All these requirements can be fulfilled by the concept presented in this paper.

The case study shows that the more methods used, the better the interpretation of the geological structure of the landslide, especially in cases where additional triggering occurs. For valid interpretation of geophysical results, all data should be verified. The presented approach, although applied to a specific case, can be an example, where with a lack of borehole information, the reliability of the result can be estimated. The ERT measurements led to the approximation of the shape of geological structures. MASW enabled the distinction of layers near the surface, while SRT helped to distinguish successive geological layers. The created high-resolution DTM models, in combination with geophysical methods, allowed a more comprehensive picture of the landslide structure to be created, increasing the possibility of interpretation and data comparison. The methodology was applied to a landslide where previous studies had been conducted to compare the evolution of ground movement over time. The analysis of the results supported by the detailed uncertainty analysis allowed tracking the temporal changes of the rupture surface and colluvium in a case of seasonal and anthropogenically triggering landslide.

The work presented here provides a valuable framework for further studies of unstable slopes, through a multimethod concept. Nevertheless, it is also recommended that geological drilling should be carried out to finally integrate geological data with geophysical imaging. As the study of landslides requires a holistic approach, further imaging of landslide changes is necessary, especially using the latest geophysical imaging methods.

Author Contributions: Conceptualization, A.M. and I.S.-K.; methodology, M.W., I.S.-K. and A.N.; software, A.M., I.S.-K., M.M. and A.N.; validation, J.C., M.M. and S.K.; formal analysis, M.W. and S.K.; investigation, M.W., A.M., S.K., I.S.-K. and A.N.; resources, S.K., I.S.-K., M.M. and A.N.; data curation, A.M., S.K. and M.W.; writing—original draft preparation, M.W., I.S.-K., A.M., M.M., S.K., A.N. and J.C.; writing—review and editing, J.C. and M.W.; visualization, M.W., I.S.-K., A.M., A.N. and J.C.; supervision, I.S.-K., A.M., M.M. and S.K.; project administration, A.M.; funding acquisition, A.M. All authors have read and agreed to the published version of the manuscript.

Funding: This research was funded by the National Science Centre, Poland (NCN), grant number 2020/37/N/ST10/01486.

Data Availability Statement: The data presented in this study are available on request from the corresponding author.

Acknowledgments: We thank Brij Singh, Bartosz Owoc, and Mariusz Chmielewski for helping during data acquisition. Map data copyrighted OpenStreetMap contributors and available from <https://www.openstreetmap.org>, accessed on 12 October 2022 (Figure 1a).

Conflicts of Interest: The authors declare no conflict of interest.

References

- Pasierb, B.; Grodecki, M.; Gwóźdź, R. Geophysical and Geotechnical Approach to a Landslide Stability Assessment: A Case Study. *Acta Geophys.* **2019**, *67*, 1823–1834. [[CrossRef](#)]
- Gariano, S.L.; Guzzetti, F. Landslides in a Changing Climate. *Earth Sci. Rev.* **2016**, *162*, 227–252. [[CrossRef](#)]
- Ilcewicz-Stefaniuk, D.; Lemberger, M.; Magiera, J.; Rybicki, S.; Słomka, T.; Stefaniuk, M. Cataloguing Natural Geological Hazards over Poland's Territory. *Polish Geol. Inst. Spec. Pap.* **2004**, *15*, 53–60.
- Jaboyedoff, M.; Michoud, C.; Derron, M.-H.; Voumard, J.; Leibundgut, G.; Sudmeier-Rieux, K.; Nadim, F.; Leroi, E. Human-Induced Landslides: Toward the Analysis of Anthropogenic Changes of the Slope Environment. In *Landslides and Engineered Slopes—Experience, Theory and Practice: Proceedings of the 12th International Symposium on Landslides*; Aversa, S., Cascini, L., Picarelli, L., Scavia, C., Eds.; CRC Press: London, UK, 2016; pp. 217–232, ISBN 9781138029880.
- Wójcik, A.; Wójciechowski, T. Landslides as One of the Most Important Elements of Geological Hazards in Poland. *Prz. Geol.* **2016**, *64*, 701–709. (In Polish)
- Petley, D. Global Patterns of Loss of Life from Landslides. *Geology* **2012**, *40*, 927–930. [[CrossRef](#)]
- Israil, M.; Pachauri, A.K. Geophysical Characterization of a Landslide Site in the Himalayan Foothill Region. *J. Asian Earth Sci.* **2003**, *22*, 253–263. [[CrossRef](#)]
- Kos, J.; Wójcik, A. Geological and Engineering Documentation of Landslides in the Carpathian Flysch. *Prz. Geol.* **2021**, *69*, 825–834. (In Polish) [[CrossRef](#)]
- Wojciechowski, T. Landslide Susceptibility of Poland. *Prz. Geol.* **2019**, *67*, 320–325. (In Polish) [[CrossRef](#)]
- Marciniak, P.; Zimnal, Z.; Wojciechowski, T.; Perski, Z.; Rczkowski, W.; Laskowicz, I.; Nescieruk, P.; Grabowski, D.; Kuak, M.; Wójcik, A. Landslides in Poland: From Registration to Forecast, 13 Years of the LCS Project. *Prz. Geol.* **2019**, *67*, 291–297. (In Polish)
- Poprawa, D.; Rączkowski, W. Carpathian Landslides (Southern Poland). *Prz. Geol.* **2003**, *51*, 685–692. (In Polish)
- Corominas, J.; van Westen, C.; Frattini, P.; Cascini, L.; Malet, J.P.; Fotopoulou, S.; Catani, F.; Van Den Eeckhaut, M.; Mavrouli, O.; Agliardi, F.; et al. Recommendations for the Quantitative Analysis of Landslide Risk. *Bull. Eng. Geol. Environ.* **2014**, *73*, 209–263. [[CrossRef](#)]
- Zhong, C.; Liu, Y.; Gao, P.; Chen, W.; Li, H.; Hou, Y.; Nuremanguli, T.; Ma, H. Landslide Mapping with Remote Sensing: Challenges and Opportunities. *Int. J. Remote Sens.* **2020**, *41*, 1555–1581. [[CrossRef](#)]
- Mohan, A.; Singh, A.K.; Kumar, B.; Dwivedi, R. Review on Remote Sensing Methods for Landslide Detection Using Machine and Deep Learning. *Trans. Emerg. Telecommun. Technol.* **2021**, *32*, e3998. [[CrossRef](#)]
- Travelletti, J.; Demand, J.; Jaboyedoff, M.; Marillier, F. Mass Movement Characterization Using a Reflexion and Refraction Seismic Survey with the Sloping Local Base Level Concept. *Geomorphology* **2010**, *116*, 1–10. [[CrossRef](#)]
- El-Raouf, A.A.; Iqbal, I.; Meister, J.; Abdelrahman, K.; Alzahrani, H.; Badran, O.M. Earthflow Reactivation Assessment by Multichannel Analysis of Surface Waves and Electrical Resistivity Tomography: A Case Study. *Open Geosci.* **2021**, *13*, 1328–1344. [[CrossRef](#)]
- Whiteley, J.S.; Watlet, A.; Uhlemann, S.; Wilkinson, P.; Boyd, J.P.; Jordan, C.; Kendall, J.M.; Chambers, J.E. Rapid Characterisation of Landslide Heterogeneity Using Unsupervised Classification of Electrical Resistivity and Seismic Refraction Surveys. *Eng. Geol.* **2021**, *290*, 106189. [[CrossRef](#)]
- Casagli, N.; Cigna, F.; Bianchini, S.; Hölbling, D.; Füreder, P.; Righini, G.; Del Conte, S.; Friedl, B.; Schneiderbauer, S.; Iasio, C.; et al. Landslide Mapping and Monitoring by Using Radar and Optical Remote Sensing: Examples from the EC-FP7 Project SAFER. *Remote Sens. Appl. Soc. Environ.* **2016**, *4*, 92–108. [[CrossRef](#)]
- Lissak, C.; Bartsch, A.; De Michele, M.; Gomez, C.; Maquaire, O.; Raucoules, D.; Roulland, T. Remote Sensing for Assessing Landslides and Associated Hazards. *Surv. Geophys.* **2020**, *41*, 1391–1435. [[CrossRef](#)]
- Carlà, T.; Tofani, V.; Lombardi, L.; Raspini, F.; Bianchini, S.; Bertolo, D.; Thuegaz, P.; Casagli, N. Combination of GNSS, Satellite InSAR, and GBInSAR Remote Sensing Monitoring to Improve the Understanding of a Large Landslide in High Alpine Environment. *Geomorphology* **2019**, *335*, 62–75. [[CrossRef](#)]
- Arabameri, A.; Pradhan, B.; Rezaei, K.; Lee, C.W. Assessment of Landslide Susceptibility Using Statistical- and Artificial Intelligence-Based FR-RF Integrated Model and Multiresolution DEMs. *Remote Sens.* **2019**, *11*, 999. [[CrossRef](#)]
- Hong, H.; Pradhan, B.; Jebur, M.N.; Bui, D.T.; Xu, C.; Akgun, A. Spatial Prediction of Landslide Hazard at the Luxi Area (China) Using Support Vector Machines. *Environ. Earth Sci.* **2016**, *75*, 40. [[CrossRef](#)]

23. Ghorbanzadeh, O.; Blaschke, T.; Gholamnia, K.; Meena, S.R.; Tiede, D.; Aryal, J. Evaluation of Different Machine Learning Methods and Deep-Learning Convolutional Neural Networks for Landslide Detection. *Remote Sens.* **2019**, *11*, 196. [[CrossRef](#)]
24. Svennevig, K. Preliminary Landslide Mapping in Greenland. *Geol. Surv. Denmark Greenl. Bull.* **2019**, *43*, 1–5. [[CrossRef](#)]
25. Ciampalini, A.; Raspini, F.; Bianchini, S.; Frodella, W.; Bardi, F.; Lagomarsino, D.; Di Traglia, F.; Moretti, S.; Proietti, C.; Pagliara, P.; et al. Remote Sensing as Tool for Development of Landslide Databases: The Case of the Messina Province (Italy) Geodatabase. *Geomorphology* **2015**, *249*, 103–118. [[CrossRef](#)]
26. Grima, N.; Edwards, D.; Edwards, F.; Petley, D.; Fisher, B. Landslides in the Andes: Forests Can Provide Cost-Effective Landslide Regulation Services. *Sci. Total Environ.* **2020**, *745*, 141128. [[CrossRef](#)]
27. Strozzi, T.; Klimeš, J.; Frey, H.; Caduff, R.; Huggel, C.; Wegmüller, U.; Rapre, A.C. Satellite SAR Interferometry for the Improved Assessment of the State of Activity of Landslides: A Case Study from the Cordilleras of Peru. *Remote Sens. Environ.* **2018**, *217*, 111–125. [[CrossRef](#)]
28. Aslan, G.; Fomelis, M.; Raucoules, D.; De Michele, M.; Bernardie, S.; Cakir, Z. Landslide Mapping and Monitoring Using Persistent Scatterer Interferometry (PSI) Technique in the French Alps. *Remote Sens.* **2020**, *12*, 1305. [[CrossRef](#)]
29. Kang, Y.; Zhao, C.; Zhang, Q.; Lu, Z.; Li, B. Application of InSAR Techniques to an Analysis of the Guanling Landslide. *Remote Sens.* **2017**, *9*, 1046. [[CrossRef](#)]
30. Pawluszek-Filipiak, K.; Borkowski, A.; Motagh, M. Multi-Temporal Landslide Activity Investigation by Spaceborne SAR Interferometry: The Case Study of the Polish Carpathians. *Remote Sens. Appl. Soc. Environ.* **2021**, *24*, 100629. [[CrossRef](#)]
31. Hussain, Y.; Schlögel, R.; Innocenti, A.; Hamza, O.; Iannucci, R.; Martino, S.; Havenith, H. Review on the Geophysical and UAV-Based Methods Applied to Landslides. *Remote Sens.* **2022**, *14*, 4564. [[CrossRef](#)]
32. Kamiński, M.; Zientara, P.; Krawczyk, M. Electrical Resistivity Tomography and Digital Aerial Photogrammetry in the Research of the “Bachledzki Hill” Active Landslide—In Podhale (Poland). *Eng. Geol.* **2021**, *285*, 106004. [[CrossRef](#)]
33. Karwacki, K. Use of Aerial Images in Research of Mass Movements—A Case Study of the Lachowice Landslide (Western Carpathians, Beskid Makowski Mts). *Biul. Państw. Inst. Geol.* **2016**, *466*, 115–122. [[CrossRef](#)]
34. Perski, Z.; Wojciechowski, T.; Wójcik, A.; Borkowski, A. Monitoring of Landslide Dynamics with SAR Interferometry and LIDAR. Case Study of Klodne Landslide (Southern Poland). In Proceedings of the 3rd World Landslide Forum, Beijing, China, 2–6 June 2014.
35. Zygumt, M.; Sanecki, J.; Klewski, A. Determination of the Causes of Landslides in the Polish Flysch Carpathians Based on UAV Aerial Images. *J. Civ. Eng. Environ. Archit.* **2017**, *34*, 413–422. (In Polish) [[CrossRef](#)]
36. Prokešová, R.; Kardoš, M.; Medved'ová, A. Landslide Dynamics from High-Resolution Aerial Photographs: A Case Study from the Western Carpathians, Slovakia. *Geomorphology* **2010**, *115*, 90–101. [[CrossRef](#)]
37. Wojciechowski, T.; Borkowski, A.; Perski, Z.; Wójcik, A. Airborne Laser Scanning Data in Landslide Studies at the Example Of the Zbyszyce Landslide (Outer Carpathians). *Prz. Geol.* **2012**, *60*, 95–102. (In Polish)
38. Stumpf, A.; Malet, J.P.; Allemand, P.; Pierrot-Deseilligny, M.; Skupinski, G. Ground-Based Multi-View Photogrammetry for the Monitoring of Landslide Deformation and Erosion. *Geomorphology* **2015**, *231*, 130–145. [[CrossRef](#)]
39. Bitelli, G.; Dubbini, M.; Zanutta, A.; Scanning, L.; Sensing, R. Terrestrial Laser Scanning and Digital Photogrammetry Techniques To Monitor Landslide Bodies. In Proceedings of the 20th ISPRS Congress Geo-Imagery Bridging Continents, Istanbul, Turkey, 12–23 July 2004; pp. 246–251.
40. Travelletti, J.; Delacourt, C.; Allemand, P.; Malet, J.P.; Schmittbuhl, J.; Toussaint, R.; Bastard, M. Correlation of Multi-Temporal Ground-Based Optical Images for Landslide Monitoring: Application, Potential and Limitations. *ISPRS J. Photogramm. Remote Sens.* **2012**, *70*, 39–55. [[CrossRef](#)]
41. Corsini, A.; Farina, P.; Antonello, G.; Barbieri, M.; Casagli, N.; Coren, F.; Guerri, L.; Ronchetti, F.; Sterzai, P.; Tarchi, D. Space-Borne and Ground-Based SAR Interferometry as Tools for Landslide Hazard Management in Civil Protection. *Int. J. Remote Sens.* **2006**, *27*, 2351–2369. [[CrossRef](#)]
42. Wang, G.; Joyce, J.; Phillips, D.; Shrestha, R.; Carter, W. Delineating and Defining the Boundaries of an Active Landslide in the Rainforest of Puerto Rico Using a Combination of Airborne and Terrestrial LIDAR Data. *Landslides* **2013**, *10*, 503–513. [[CrossRef](#)]
43. Baltensweiler, A.; Walthert, L.; Ginzler, C.; Sutter, F.; Purves, R.S.; Hanewinkel, M. Terrestrial Laser Scanning Improves Digital Elevation Models and Topsoil PH Modelling in Regions with Complex Topography and Dense Vegetation. *Environ. Model. Softw.* **2017**, *95*, 13–21. [[CrossRef](#)]
44. Pilecka, E. Remote Sensing as the Method for Analysis of Mass Movements. *Bull. Miner. Energy Econ. Res. Inst. Polish Acad. Sci.* **2013**, *84*, 103–115.
45. Bruno, F.; Martillier, F. Test of High-Resolution Seismic Reflection and Other Geophysical Techniques on the Boup Landslide in the Swiss Alps. *Surv. Geophys.* **2000**, *21*, 333–348. [[CrossRef](#)]
46. Eichkitz, C.G.; Schreilechner, M.G.; Amtmann, J.; Schmid, C. Shallow Seismic Reflection Study of the Gschlifgraben Landslide Deposition Area—Interpretation and Three Dimensional Modeling. *Austrian J. Earth Sci.* **2009**, *102*, 52–60.
47. Wang, S.; Malehmir, A.; Bastani, M. Geophysical Characterization of Areas Prone to Quick-Clay Landslides Using Radio-Magnetotelluric and Seismic Methods. *Tectonophysics* **2016**, *677–678*, 248–260. [[CrossRef](#)]
48. Renalier, F.; Jongmans, D.; Campillo, M.; Bard, P.Y. Shear Wave Velocity Imaging of the Avignonet Landslide (France) Using Ambient Noise Cross Correlation. *J. Geophys. Res. Earth Surf.* **2010**, *115*, F03032. [[CrossRef](#)]

49. Lapenna, V.; Lorenzo, P.; Perrone, A.; Piscitelli, S.; Rizzo, E.; Sdao, F. 2D Electrical Resistivity Imaging of Some Complex Landslides in the Lucanian Apennine Chain, Southern Italy. *Geophysics* **2005**, *70*, B11. [[CrossRef](#)]
50. Bellanova, J.; Calamita, G.; Giocoli, A.; Luongo, R.; Macchiato, M.; Perrone, A.; Uhlemann, S.; Piscitelli, S. Electrical Resistivity Imaging for the Characterization of the Montaguto Landslide (Southern Italy). *Eng. Geol.* **2018**, *243*, 272–281. [[CrossRef](#)]
51. Bednarczyk, Z. Application of GPR Scanning for Landslide Investigations in Polish Carpathians. In Proceedings of the Near Surface 2008-14th EAGE European Meeting of Environmental and Engineering Geophysics, Krakow, Poland, 15–17 September 2008; pp. 372–376.
52. Borecka, A.; Herzig, J.; Durjasz-Rybacka, M. Ground Penetrating Radar Investigations of Landslides: A Case Study in a Landslide in Radziszów. *Stud. Geotech. Mech.* **2015**, *37*, 11–18. [[CrossRef](#)]
53. Kowalczyk, S.; Mieszkowski, R.; Pacanowski, G. The Stability Evaluation of Warsaw Slope Selected Pieces Based on Electrical Resistivity Tomography Survey (ERT). *Przegląd Geol.* **2014**, *62*, 634–640. (In Polish)
54. Orozco, A.F.; Bücker, M.; Steiner, M.; Malet, J.P. Complex-Conductivity Imaging for the Understanding of Landslide Architecture. *Eng. Geol.* **2018**, *243*, 241–252. [[CrossRef](#)]
55. Mreyen, A.-S.; Cauchie, L.; Micu, M.; Onaca, A.; Havenith, H.-B. Multiple Geophysical Investigations to Characterize Massive Slope Failure Deposits: Application to the Balta Rockslide, Carpathians. *Geophys. J. Int.* **2021**, *225*, 1032–1047. [[CrossRef](#)]
56. Bichler, A.; Bobrowsky, P.; Best, M.; Douma, M.; Hunter, J.; Calvert, T.; Burns, R. Three-Dimensional Mapping of a Landslide Using a Multi-Geophysical Approach: The Quesnel Forks Landslide. *Landslides* **2004**, *1*, 29–40. [[CrossRef](#)]
57. Mantovani, M.; Devoto, S.; Forte, E.; Mocnik, A.; Pasuto, A.; Piacentini, D.; Soldati, M. A Multidisciplinary Approach for Rock Spreading and Block Sliding Investigation in the North-Western Coast of Malta. *Landslides* **2013**, *10*, 611–622. [[CrossRef](#)]
58. Godio, A.; Strobbia, C.; De Bacco, G. Geophysical Characterisation of a Rockslide in an Alpine Region. *Eng. Geol.* **2006**, *83*, 273–286. [[CrossRef](#)]
59. Khan, M.A.; Basharat, M.; Riaz, M.T.; Sarfraz, Y.; Farooq, M.; Khan, A.Y.; Pham, Q.B.; Ahmed, K.S.; Shahzad, A. An Integrated Geotechnical and Geophysical Investigation of a Catastrophic Landslide in the Northeast Himalayas of Pakistan. *Geol. J.* **2021**, *56*, 4760–4778. [[CrossRef](#)]
60. Bogoslovsky, V.A.; Ogilvy, A.A. Geophysical Methods for the Investigation of Landslides. *Geophysics* **1977**, *42*, 562–571. [[CrossRef](#)]
61. Bestyński, Z. Geophysical Methods in Engineering Geology. *Biul. PIG* **2011**, *446*, 175–182. (In Polish)
62. Ostrowski, S.; Pacanowski, G.; Lasocki, M. Application of Engineering Geophysics Methods to Recognize the Genesis of Carpathian Landslides. *Biul. Inf. Geofiz.* **2011**, *10*, 19–25. (In Polish)
63. Bestyński, Z.; Pacanowski, G.; Sieński, E. Geophysical Investigation and Geotechnical Classifications for Stability Assessment of Carpathian Flysch Slopes. *Prz. Geol.* **2017**, *65*, 717–724. (In Polish)
64. Crawford, M.M.; Bryson, L.S.; Woolery, E.W.; Wang, Z. Using 2-D Electrical Resistivity Imaging for Joint Geophysical and Geotechnical Characterization of Shallow Landslides. *J. Appl. Geophys.* **2018**, *157*, 37–46. [[CrossRef](#)]
65. Marciniak, A.; Kowalczyk, S.; Gontar, T.; Owoc, B.; Nawrot, A.; Luks, B.; Cader, J.; Majdański, M. Integrated Geophysical Imaging of a Mountain Landslide—A Case Study from the Outer Carpathians, Poland. *J. Appl. Geophys.* **2021**, *191*, 104364. [[CrossRef](#)]
66. Gawriuczenkow, I.; Kaczmarek, Ł.; Kielbasiński, K.; Kowalczyk, S.; Mieszkowski, R.; Wójcik, E. Slope Stability and Failure Hazards in the Light of Complex Geological Surveys. *Sci. Rev. Eng. Environ. Sci.* **2017**, *26*, 85–98. (In Polish) [[CrossRef](#)]
67. Whiteley, J.S.; Chambers, J.E.; Uhlemann, S.; Wilkinson, P.B.; Kendall, J.M. Geophysical Monitoring of Moisture-Induced Landslides: A Review. *Rev. Geophys.* **2019**, *57*, 106–145. [[CrossRef](#)]
68. Danneels, G.; Bourdeau, C.; Torgoev, I.; Havenith, H.B. Geophysical Investigation and Dynamic Modelling of Unstable Slopes: Case-Study of Kainama (Kyrgyzstan). *Geophys. J. Int.* **2008**, *175*, 17–34. [[CrossRef](#)]
69. Tsai, W.N.; Chen, C.C.; Chiang, C.W.; Chen, P.Y.; Kuo, C.Y.; Wang, K.L.; Lin, M.L.; Chen, R.F. Electrical Resistivity Tomography (ERT) Monitoring for Landslides: Case Study in the Lantai Area, Yilan Taiping Mountain, Northeast Taiwan. *Front. Earth Sci.* **2021**, *9*, 1–17. [[CrossRef](#)]
70. Oldenborger, G.A.; Knoll, M.D.; Routh, P.S.; LaBrecque, D.J. Time-Lapse ERT Monitoring of an Injection/Withdrawal Experiment in a Shallow Unconfined Aquifer. *Geophysics* **2007**, *72*, F177. [[CrossRef](#)]
71. Nolet, G. *A Breviary of Seismic Tomography: Imaging the Interior of the Earth and Sun*; Cambridge University Press: Cambridge, UK, 2008.
72. Wood, C.M.; Cox, B.R. A Comparison of MASW Dispersion Uncertainty and Bias for Impact and Harmonic Sources. In Proceedings of the GeoCongress 2012, Oakland, CA, USA, 25–29 March 2012; pp. 2756–2765.
73. Zhao, C.; Lu, Z. Remote Sensing of Landslides—A Review. *Remote Sens.* **2018**, *10*, 279. [[CrossRef](#)]
74. Kniess, U.; Travalletti, J.; Daehne, A.; Krzeminska, D.; Bièvre, G.; Jongmans, D.; Corsini, A.; Bogaard, T.; Malet, J.-P. Innovative Techniques for the Characterization of the Morphology, Geometry and Hydrological Features of Slow-Moving Landslides. In *Mountain Risks: From Prediction to Management and Governance*; Van Asch, T., Corominas, J., Greiving, S., Malet, J.-P., Sterlacchini, S., Eds.; Springer: Dordrecht, The Netherlands, 2014; pp. 57–82, ISBN 978-94-007-6769-0.
75. Lapenna, V.; Guariglia, A.; Saladino, R.; Arbia, F.; Lacovara, B.; Perrone, A.; Simoniello, T. Airborne Laser Scanner, Optical High-Resolution Images Analysis and Geophysical Survey for Investigating the Slope of Bosco Piccolo Village (Basilicata Region, Southern Italy). In Proceedings of the EGU General Assembly Conference Abstracts, Vienna, Austria, 19–24 April 2009; p. 12975.
76. Travalletti, J.; Malet, J.P. Characterization of the 3D Geometry of Flow-like Landslides: A Methodology Based on the Integration of Heterogeneous Multi-Source Data. *Eng. Geol.* **2012**, *128*, 30–48. [[CrossRef](#)]

77. Çelik, S.; Özyazıcıoğlu, M.; Şahin, R.; Uysal, H.; Çakıcı, F.Z.; Kalkan, E. The Destruction of Erzurum Ski-Jumping Complex by a Landslide: Evaluation of an Engineering Design Failure. *Nat. Hazards* **2021**, *107*, 475–496. [CrossRef]
78. Dankers, R.; Feyen, L. Climate Change Impact on Flood Hazard in Europe: An Assessment Based on High-Resolution Climate Simulations. *J. Geophys. Res. Atmos.* **2008**, *113*, D19105. [CrossRef]
79. Twardosz, R.; Walanus, A.; Guzik, I. Warming in Europe: Recent Trends in Annual and Seasonal Temperatures. *Pure Appl. Geophys.* **2021**, *178*, 4021–4032. [CrossRef]
80. Lollino, P.; Cotecchia, F.; Elia, G.; Mitaritonna, G.; Santalucia, F. Interpretation of Landslide Mechanisms Based on Numerical Modelling: Two Case-Histories. *Eur. J. Environ. Civ. Eng.* **2014**, *20*, 1032–1053. [CrossRef]
81. Meusbürger, K.; Alewell, C. Impacts of Anthropogenic and Environmental Factors on the Occurrence of Shallow Landslides in an Alpine Catchment (Urseren Valley, Switzerland). *Nat. Hazards Earth Syst. Sci.* **2008**, *8*, 509–520. [CrossRef]
82. Glade, T. Landslide Occurrence as a Response to Land Use Change: A Review of Evidence from New Zealand. *Catena* **2003**, *51*, 297–314. [CrossRef]
83. Soldati, M.; Corsini, A.; Pasuto, A. Landslides and Climate Change in the Italian Dolomites since the Late Glacial. *Catena* **2004**, *55*, 141–161. [CrossRef]
84. Borgatti, L.; Soldati, M. Landslides as a Geomorphological Proxy for Climate Change: A Record from the Dolomites (Northern Italy). *Geomorphology* **2010**, *120*, 56–64. [CrossRef]
85. Froude, M.J.; Petley, D.N. Global Fatal Landslide Occurrence from 2004 to 2016. *Nat. Hazards Earth Syst. Sci.* **2018**, *18*, 2161–2181. [CrossRef]
86. Marciniak, A.; Stan-Kłeczek, I.; Idziak, A.; Majdański, M. Uncertainty Based Multi-Step Seismic Analysis for near-Surface Imaging. *Open Geosci.* **2019**, *11*, 727–737. [CrossRef]
87. OpenStreetMap Contributors Planet Dump [Data File from 06.09.2022]. Available online: <https://planet.openstreetmap.org> (accessed on 6 September 2022).
88. Paul, Z.; Ryłko, W.; Tomasz, A. Zarys Budowy Geologicznej Zachodniej Części Karpat Polskich (Bez Utworów Czwartorzędowych). *Prz. Geol.* **1996**, *44*, 469–476. (In Polish)
89. Cieszkowski, M.; Golonka, J.; Krobicki, M.; Ślącza, A.; Waśkowska, A.; Wendorf, M. Olistoliths within the Silesian Series and Their Connections with Evolutionary Stages of the Silesian Basin. *Geologia* **2009**, *35*, 13–21. (In Polish)
90. Waśkowska-Oliwa, A. The Eocene Hieroglyphic Beds and Green Shales in the Rożnów Lake Area (Silesian Nappe, Outer Carpathians)—Facies Development and Biostratigraphy. *Geol. Geophys. Environ.* **2014**, *40*, 5–26. [CrossRef]
91. Golonka, J.; Waśkowska-Oliwa, A. Stratigraphy of the Polish Flysch Carpathians between Bielsko-Biała and Nowy Targ. *Geol. Akad. Górniczo-Hut. Im. Stanisława Staszica W Krakowie* **2007**, *33*, 5–27. (In Polish)
92. Cieszkowski, M.; Golonka, J.; Waśkowska-Oliwa, A.; Chrutek, M. Geological Structure of the Sucha Beskidzka Region—Świnna Poreba (Polish Flysch Carpathians). *Kwart. AGH Geol.* **2006**, *32*, 155–201. (In Polish)
93. PGI-NRI Geological Map of Poland 1:50000. Available online: <https://geologia.pgi.gov.pl/arcgis/apps/MapSeries> (accessed on 7 November 2022).
94. Bestyński, Z.; Thiel, K. Geophysical Investigations of the Carpathian Slide Slopes. *Polish Geol. Inst. Spec. Pap.* **2005**, *20*, 35–39.
95. Pilecki, Z.; Zietek, J.; Karczewski, J.; Pilecka, E.; Klosinski, J. The Effectiveness of Recognizing of Failure Surface of the Carpathian Flysch Landslide Using Wave Methods. In Proceedings of the Near Surface 2007—13th European Meeting of Environmental and Engineering Geophysics, Istanbul, Turkey, 3–5 September 2007; pp. 256–260.
96. Ostrowski, S.; Rybak-Ostrowska, B.; Lasocki, M. Application of Near-Surface Geophysical Survey for Recognition of the Geology of Landslide Areas in the Carpathians—A Case Study. *Prz. Geol.* **2013**, *61*, 67–73. (In Polish)
97. Leica Geosystems Leica Viva GPS RTK—Instrument Datasheet. Available online: <https://leica-geosystems.com/en-us/products/gnss-systems/controllers/leica-viva-cs15-and-cs10#> (accessed on 20 December 2022).
98. Guideline Geo ABEM Terrameter LS—Instrument Datasheet. Available online: <https://www.guidelinegeoc.cdn.triggerfish.cloud/uploads/2016/11/ABEM-Terrameter-LS-Technical-Specifications.pdf> (accessed on 20 December 2022).
99. Guideline Geo ABEM Terraloc—Instrument Datasheet. Available online: <https://www.guidelinegeoc.cdn.triggerfish.cloud/uploads/2017/07/ABEM-Terraloc-Pro-2-TechSpec-210823-web.pdf> (accessed on 20 December 2022).
100. RIEGL RIEGL VZ 6000—Instrument Datasheet. Available online: http://www.riegl.com/uploads/tx_pxpriegldownloads/RIEGL_VZ-6000_Datasheet_2020-09-14.pdf (accessed on 20 December 2022).
101. GUGiK ASG-EUPOS System. Available online: <http://www.asgeupos.pl> (accessed on 20 December 2022).
102. Loke, M.H. *Tutorial: 2-D and 3-D Electrical Imaging Surveys*; Geotomo Software: Gelugor, Malaysia, 2018.
103. Park, C.B.; Miller, R.D.; Miura, H. Optimum Field Parameters of an MASW Survey. *Proc. Soc. Explor. Geophys. Jpn. Tokyo* **2002**, *22*, 23.
104. Pilecki, Z. Techniki Sejsmiczne. In *Metoda Sejsmiczna w Geoinżynierii*; IGSMiE PAN: Kraków, Poland, 2018; pp. 123–168, ISBN 9788362922895. (In Polish)
105. Dal Moro, G. (Ed.) *Surface Wave Analysis for Near Surface Applications*; Elsevier: Oxford, UK, 2014; ISBN 978-0-12-800770-9.
106. Bohlen, T. Parallel 3-D Viscoelastic Finite Difference Seismic Modelling. *Comput. Geosci.* **2002**, *28*, 887–899. [CrossRef]

107. de Jong, C.; Carletti, G.; Previtali, F. Assessing Impacts of Climate Change, Ski Slope, Snow and Hydraulic Engineering on Slope Stability in Ski Resorts (French and Italian Alps). In *Engineering Geology for Society and Territory—Volume 1*; Lollino, G., Manconi, A., Clague, J., Shan, W., Chiarle, M., Eds.; Springer International Publishing: Cham, Switzerland, 2015; pp. 51–55, ISBN 978-3-319-09300-0.
108. Matsuura, S.; Okamoto, T.; Osawa, H.; Shibasaki, T.; Abe, K.; Okada, Y. Fluctuations in the Pore-Water Pressure of a Reactivated Landslide in a Snowy District. In *Landslide Science for a Safer Geoenvironment Vol. 3 Targeteted Landslides*; Springer: Cham, Switzerland, 2014; Volume 3, pp. 1–717. [[CrossRef](#)]
109. Kawagoe, S.; Kazama, S.; Sarukkalige, P.R. Assessment of Snowmelt Triggered Landslide Hazard and Risk in Japan. *Cold Reg. Sci. Technol.* **2009**, *58*, 120–129. [[CrossRef](#)]
110. Yalcinkaya, E.; Alp, H.; Ozel, O.; Gorgun, E.; Martino, S.; Lenti, L.; Bourdeau, C.; Bigarre, P.; Coccia, S. Near-Surface Geophysical Methods for Investigating the Buyukcekmece Landslide in Istanbul, Turkey. *J. Appl. Geophys.* **2016**, *134*, 23–35. [[CrossRef](#)]

Disclaimer/Publisher’s Note: The statements, opinions and data contained in all publications are solely those of the individual author(s) and contributor(s) and not of MDPI and/or the editor(s). MDPI and/or the editor(s) disclaim responsibility for any injury to people or property resulting from any ideas, methods, instructions or products referred to in the content.